First posted online on 15 June 2020 as 10.1242/dmm.044420
Access the most recent version at http://dmm.biologists.org/lookup/doi/10.1242/dmm.044420

A *Drosophila* model of oral peptide therapeutics for adult Intestinal Stem Cell tumors

Anjali Bajpai[1*], Quazi Taushif Ahmad[1], Hong-Wen Tang[2], Nishat Manzar[1], Virender Singh[1,4], Ashwani Thakur[1], Bushra Ateeq[1], Norbert Perrimon[2,3], Pradip Sinha[1*]

[1]Biological Sciences and Bioengineering, Indian Institute of Technology Kanpur, Kanpur, India.

[2]Department of Genetics, Blavatnik Institute, Harvard Medical School, Boston, MA 02115, USA.

[3]Howard Hughes Medical Institute, Boston, MA 02115, USA.

[4]Department of Physiology & Biophysics, Case Western Reserve University, Cleveland, OH 44106.

*Authors for correspondence: anjalii@iitk.ac.in, pradips@iitk.ac.in

Key words: *Drosophila*, Peptide therapeutic, Yki, Intestinal Stem Cells, Integrin signaling

SUMMARY STATEMENT

We demonstrate that when fed to flies, TONDU peptide suppresses Yki-driven Intestinal Stem Cell (ISC) tumors, and identify integrins as essential components of ISC tumorigenesis.

ABSTRACT

Peptide therapeutics, unlike small molecule drugs, display crucial advantages of target-specificity and the ability to block large interacting interfaces such as those of transcription factors. The transcription co-factor of the Hippo pathway, YAP/Yki, has been implicated in many cancers, and is dependent on its interaction with the DNA-binding TEAD/Sd proteins via a large Ω-loop. In addition, the mammalian Vestigial Like (VGLL) protein, specifically its TONDU domain, competitively inhibits YAP-TEAD interaction, resulting in arrest of tumor growth. Here, we show that either overexpression of the TONDU peptide or its oral uptake leads to suppression of Yorkie (Yki)-driven intestinal stem cell (ISC) tumors in the adult *Drosophila* midgut. In addition, comparative proteomic analyses of peptide-treated and untreated tumors, together with ChIP analysis, reveal that integrin pathway members are part of the Yki-oncogenic network. Collectively, our findings establish *Drosophila* as a reliable *in vivo* platform to screen for cancer oral therapeutic peptides and reveal a tumor suppressive role for integrins in Yki-driven tumors.

INTRODUCTION

Drosophila has emerged as an effective tumor model for the screening of small molecule therapeutics (Dar et al., 2012; Khoo et al., 2013; Markstein et al., 2014; Bangi et al., 2016). Whereas cancer-promoting misregulated kinases are amenable to inhibition by small molecules, others, such as transcription factors and co-factors, are largely considered undruggable (Bhagwat and Vakoc, 2015; Lambert et al., 2018). In this regard, peptides are particularly attractive as therapeutic molecules (Lau and Dunn, 2018; Drucker, 2019) because of their high selectivity, improved tolerance, and ability to target large interacting interfaces (Furet et al., 2019). While most peptide therapeutics require parenteral injection, their oral delivery is highly desirable; indeed, currently a few orally derived therapeutic peptides are being tested in clinical trials (Drucker, 2019).

The proto-oncogene YAP (Yes-associated protein; Yorkie, Yki, in *Drosophila*)—the transcription co-factor of the Hippo pathway—interacts with its DNA-binding partner, TEAD (transcriptional enhanced associate domain, TEAD1-4; Scalloped (Sd) in *Drosophila*) (Wu et al., 2008), and is implicated in cancers (Zanconato et al., 2016). YAP binds to TEAD via an unusually large interface, the Ω-loop (Pobbati et al., 2012; Furet et al., 2019), which lacks a defined binding pocket, making it an unlikely target of inhibition by small molecules. TEAD proteins also bind to other transcriptional co-factors, such as the Vestigial Like (VGLL1-4) proteins that display a highly conserved 26 amino acid TONDU domain (Pobbati et al., 2012; Koontz et al., 2013). VGLL competitively inhibits binding of YAP and TEAD, thereby acting as a tumor suppressor (Zhang et al., 2014). Interestingly, a synthetic peptide analog of the TONDU domain of VGLL4 was found to inhibit gastric cancer growth (Jiao et al., 2014) in a mouse xenograft model.

Similar to the mammalian VGLL-TEAD-YAP partnership, *Drosophila* TONDU-containing proteins, such as Vestigial (Vg) and Tondu-domain-containing Growth Inhibitor (Tgi) interact with Sd and Yki (Guo et al., 2013; Koontz et al., 2013). Sd, when not bound to Yki, interacts with the ubiquitously expressed Tgi via the Tgi TONDU domain. The conserved interaction between Vg/Tgi with Sd-Yki in *Drosophila* therefore makes the fly a relevant platform to screen for large molecule inhibitors of YAP-TEAD interaction. Here, we used the adult *Drosophila* gut—which displays Sd-dependent Yki activity for intestinal stem cell (ISC) homeostasis (Jin et al., 2013)—to test whether a TONDU peptide can suppress ISC tumors triggered by a gain of an activated form of Yki (Kwon et al., 2015; Song et al., 2019).

We show that ISC tumors in the adult midgut induced by a gain of activated Yki are suppressed by feeding TONDU peptide-supplemented food. Further, comparative proteome analysis and genetic tests reveal that integrin pathway members are part of the Yki-oncogenic network. Altogether, our results establish *Drosophila* ISC tumor model as a reliable platform for screening therapeutic peptides with the added advantage of rapid resolution of the mechanistic underpinning of tumor suppression.

RESULTS

Genetic suppression of Yki-driven ISC tumor growth by the TONDU peptide

The *Drosophila* gut closely resembles the mammalian gut and is divided into the foregut, the midgut and the hindgut (Guo et al., 2016). The midgut makes up most of the gut and contains three cell types: differentiated enterocytes (ECs), entero-endocrine cells (EEs), and intestinal stem cells (ISCs) (Fig. 1A-B). Expression of a phosphorylation-defective and therefore constitutively active form of Yki in the ISCs (*esg-Gal4 Gal80^{ts}>UAS-yki^{3SA}*, referred to as *esg^{ts}>yki^{3SA}*) results in gut stem cell tumors (Kwon et al., 2015) (Fig. 1C, Fig. S1A-D). Yki gut tumor-bearing flies display a systemic wasting syndrome (Kwon et al., 2015) (Fig. 1H, Fig. S2A) and display elevated levels of the insulin antagonist *ImpL2* (Fig. 1J) (Kwon et al., 2015), in addition to canonical Yki targets (Fig. 1J) that include Sd (Fig. 1D, J), the DNA-binding partner of Yki (Wu et al., 2008).

Since the TONDU-containing proteins Vg (Khan et al., 2013) and Tgi (Guo et al., 2013; Koontz et al., 2013), can inhibit Yki-regulated growth by competing for Sd, we tested whether co-expression of TONDU peptide alone (CVVFTNYSGDTASQVDEHFSRALNY) in ISCs with gain of Yki (*esg^{ts}>yki^{3SA} UAS-vg^{TONDU}*) would inhibit Yki-driven ISC tumor growth. Indeed, a striking inhibition in ISC tumors (Fig. 1E, F) with an accompanying loss of proliferation (Fig. S2C-E) was seen under this condition. In addition, these flies showed improved life span (Fig. 1G) and a delay in the onset of tumor-associated wasting phenotypes (Fig. 1H, I and Fig S2B, F, G) with a concomitant decrease in expression of *Impl2* (Fig. 1J), a hallmark of *esg^{ts}>yki^{3SA}* tumors (Kwon et al., 2015). By contrast, overexpression of the TONDU peptide alone in ISCs (*esg^{ts}>vg^{TONDU}*) did not affect the number of ISCs (Fig. S2H, I). Altogether, these results reveal that Yki-driven ISC tumors are suppressed upon co-expression of the TONDU peptide, with an accompanying delay in the onset of tumor-associated syndromes.

Oral uptake of synthetic TONDU peptide inhibits Yki-driven ISC tumor.

Next, we asked whether feeding a synthetic TONDU peptide could inhibit Yki-driven ISC tumors comparable to its overexpression in ISCs (Fig. 1). We designed a synthetic peptide (Fig. 2A) derived from the TONDU domain of Vg that retained the conserved TEAD/Sd-interacting interfaces I and II containing the critical VXXHF motif (Pobbati et al., 2012). Further, since we aimed to administer the peptide orally to tumor bearing flies, unlike in a previous study that involved tail vein injection of VGLL4-derived peptide (Jiao et al., 2014), we tagged the TONDU peptide with an HIV-TAT motif (RKKRRQRRR) and a nuclear localizing signal (NLS) (PKKKRKV) to facilitate cellular uptake (Wadia and Dowdy, 2005) and nuclear localization, respectively. Prior to oral administration of the peptide to adult flies, we first tested cellular uptake of a fluorescent-labeled TONDU peptide in S2R+ cultured cells, and observed cytoplasmic and nuclear localization (Fig. 2B).

Further, to test whether the TONDU peptide can inhibit Yki-Sd complex formation, we used the Hippo-response-element (HRE)-luciferase reporter as a readout for Yki-Sd transcriptional activity (Wu et al., 2008). Specifically, we co-transfected S2R+ cells with the HRE-luciferase reporter along with Yki and Sd-expressing vectors, treated the cells with 100 nM of TONDU peptide, and observed a moderate but consistent decrease in luciferase activity (Fig, 2C). Next, to confirm binding of the synthetic TONDU peptide to Sd and subsequent inhibition of Yki-Sd interaction, we carried out co-immunoprecipitation studies using S2R+ cells transfected with HA-Sd and GFP-Yki in the presence of the FLAG-tagged TONDU peptide. Indeed, we found that the TONDU peptide competitively inhibits binding of Sd to Yki (Fig. 2D). Finally, when purified HA-Sd from S2R+ cells was incubated with FLAG-tagged TONDU peptide, we observed binding with Sd, as revealed by immunoblots using anti-Flag antibody (Fig. 2E). These observations are in agreement with previous studies (Guo et al., 2013; Koontz et al., 2013) that displayed binding of TONDU-containing protein Tgi to Sd via the TONDU domain. Together, these results indicate that TONDU peptide disrupts the Sd-Yki interaction by binding to Sd.

Next, we tested if oral uptake of TONDU peptide inhibits $esg^{ts}>yki^{3SA}$ ISC tumors. To first estimate the maximum tolerated dose (MTD), we examined the viability of $esg^{ts}>GFP$ flies when continuously fed different concentration (25, 50, 100, 200 and 400 µM) of the TONDU peptide in standard fly food for 6 to 10 days at 29^0C and scored their survival soon after. We observed that at 400 µM concentration of the TONDU peptide, only 55% (n=50) of the

peptide-fed *esg^{ts}>GFP* flies survived on day 6, whereas approximately 97%, 98%, 93%, and 91% (n=50 in all cases) of flies survived on 25, 50, 100 and 200 µM of the peptide, respectively. We therefore fed *esg^{ts}>yki^{3SA}* flies, 24 hours post eclosion, on 50, 100 or 200 µM of TONDU peptide-supplemented food for continuously for 10 days. Remarkably, we noted a progressive reduction in tumor load (Fig. 2F-I) with increasing concentration of TONDU peptide as seen from a decrease in the numbers of GFP-marked ISCs (Fig. 2J). By contrast, tumor load was only moderately reduced when *esg^{ts}>yki^{3SA}*flies were fed on food supplemented with sequence-scrambled TONDU peptide (Fig. S3A) at comparable concentrations (Fig. S3B-E); the residual inhibition of tumor growth observed with scrambled peptide could presumably be due to a partial retention of the secondary structure (Pobbati et al., 2012) of the TONDU peptide in the scrambled version as revealed by its predicted structure (Fig. S3F). We observed that compared to poor survival (65.6% on day 10, Fig. 1G) of untreated *esg^{ts}>yki^{3SA}* flies, TONDU peptide fed *esg^{ts}>yki^{3SA}*flies displayed consistent increase in survival (68.2%, 74.3% and 79.7%) accompanying lowering of the tumor burden (Fig. 2 G-I). We note, however, that peptide-fed flies continued to display some mortality, which we believe could be attributed to residual tumor load and/or off-target toxicity by the TONDU peptide *in vivo* due to perturbations in levels of a number of proteins in peptide-treated fly gut tumors (discussed below). Further, to confirm cellular uptake of TONDU peptide by the gut epithelia, we fed FLAG-tagged TONDU peptide (at a final concentration of 200 µM) to *esg^{ts}>yki^{3SA}* flies, and detected its cellular uptake in gut lysates by immunoblotting using an anti-FLAG antibody (Fig. S3G). In parallel, we also noted that feeding TONDU (at 200 µM) did not affect the numbers of ISCs in control guts (*esg^{ts}*>GFP) (Fig. S3H).

In addition, we tested the tumor inhibitory property of *Drosophila* TONDU peptide on human cancer cells. We observed that cell lines derived from human tumors with elevated *YAP1* levels (Fig. S3I), such as PC3 (prostate cancer), COLO-320 and WiDR (colorectal cancer), displayed growth arrest to varying extents upon uptake of TONDU peptide (Fig. 2K). On the other hand, the prostate cancer line LNCaP, which displayed negligible levels of *YAP1* (Fig. S3I), was not significantly inhibited by the TONDU peptide (Fig. 2K) even at higher concentrations, thereby revealing specificity of the TONDU peptide to inhibit YAP-mediated tumor growth and presumably low off target toxicity. Altogether, these results suggest that TONDU is therapeutically relevant in YAP-driven tumors and can effectively inhibit cancers of different tissues of origin.

Yki-driven tumor proteome reveals enrichment in integrin pathway components

We reasoned that significantly perturbed proteins in *esg^{ts}>yki^{3SA}* tumors, that are restored to normal levels following TONDU feeding are likely to represent Yki-Sd targets that are crucial to ISC tumorigenesis, and, therefore, could be therapeutically relevant. Thus, we carried out a proteome analysis using unlabeled LC-MS/MS of *esg^{ts}>yki^{3SA}* tumors on day 1 and day 7 of tumor induction**,** with or without TONDU peptide-supplemented food. Altogether, we identified 1219 proteins (including isoforms), corresponding to 2771 unique Uniprot IDs at an FDR cutoff of $q<0.05$ (Fig. 3A, Table S1) in *esg^{ts}>yki^{3SA}* tumors represented in both day 1 and day 7 ISC tumors. We next compared the proteomes of day 7 to day 1 of *esg^{ts}>yki^{3SA}* tumors, and prioritized proteins that displayed at least a $\log_2 \pm 2$ fold change (at a p value <0.05) for further analysis. Fold change was derived from the abundance measure of peptides (for a given protein) in day 7 versus day 1 of *esg^{ts}>yki^{3SA}* tumors (see methods). We identified 127 proteins (corresponding to 144 unique Uniprot IDs, including isoforms) that were differentially expressed in day 7 *esg^{ts}>yki^{3SA}* tumors, and these matched to 55 unique genes (Fig. 3B and Table S2). 45 of these showed a greater than 2-fold ($\log_2$) increase and 10 displayed a greater than 2-fold ($\log_2$) decrease in protein levels in day 7 as compared to day 1 tumors (Table S2).

To further examine whether the proteins enriched in the ISC tumors are biologically relevant, we performed a protein-protein interaction (PPI) network analysis using STRING (Szklarczyk et al., 2019); we noted significant ($p<0.001$) interaction among some of the enriched proteins (Fig. 3C) suggesting that these were not random. Furthermore, we noted that the enriched gene set included known members of the Hippo protein-protein interaction network (Kwon et al., 2013), including junction proteins Coracle, Jar, and Misshapen (Table S3). We also observed an increase in protein levels of the secreted-Wg transporter Swim (Mulligan et al., 2012). Furthermore, comparison of the day 7 proteome of *esg^{ts}>yki^{3SA}* tumors with a recently published transcriptome of *esg^{ts}>yki^{3SA}* tumors (Song et al., 2019) revealed a close correlation between changes in proteins and their respective transcript levels (r=0.548) (Fig. S4A).

Signaling pathways perturbed in tumors are often causally linked to tumor progression (see (Khan et al., 2013; Bajpai and Sinha, 2020)). We thus undertook a gene ontology (GO) classification of the proteins found enriched in ISC tumors to identify critical signaling pathways. GO classification using PANTHER (Mi et al., 2007) revealed perturbations in

several signaling pathways and protein classes (Fig. 3D and Table S4). In particular, we observed an increase in protein levels of key members of the integrin signaling pathway, including Talin (2.39 fold, all fold changes have been mentioned at $\log_2$ conversion) and the Talin-interacting adaptor proteins Vinculin (2.4 fold) and Paxillin (6.05 fold). Other members, such as αPS3 and Ilk (integrin-linked kinase), also displayed about 2-fold change, albeit at $p>0.05$ (Table S5). Consistent with these findings, we noted transcriptional upregulation of the genes encoding the integrin members in the transcriptome of comparatively aged *esg^{ts}>yki^{3SA}* tumors (Table S5, also see (Song et al., 2019)), including *mew* (αPS1), *scb* (αPS3), *mys* (βPS) and integrin-binding ligands such as LamA and LamB (Table S5) (Song et al., 2019), which were otherwise not detected in the tumor proteome (Fig. 3B). It is likely that some integrin pathway components went undetected in proteomes owing to the limitation of unlabeled LC-MS/MS such as failure to detect some proteins due to poor yield of their trypsinized products (Bantscheff et al., 2007). Significantly, we also observed an increase in levels of polarity proteins such as tight junction protein, Ferritin, Fit1, and the apical protein Shot (Fig. 3B), which are known to be regulated by the integrin pathway in the gut epithelium (Chen et al., 2018).

These observations suggest that genes encoding proteins enriched in *esg^{ts}>yki^{3SA}* tumors could be Yki-Sd transcriptional targets. To further examine this possibility, we searched for putative Yki-Sd binding sites from studies on genome-wide binding of Yki (Nagaraj et al., 2012; Oh et al., 2013) and Sd (Nagaraj et al., 2012). We noted that ~51% (23 of 45) of the genes whose protein levels were increased in *esg^{ts}>yki^{3SA}* tumors displayed putative Sd and Yki binding sites in their upstream regulatory regions (Table S6). These included several key members of the integrin pathway, including *mew, vinculin, paxillin,* and *integrin-linked kinase* and *rhea* (Fig. 3E**,** Table S6). The integrin pathway has been reported to be essential for maintenance of both ISCs (Lin et al., 2013) and Enterocytes (Chen et al., 2018); further, since αPS1 (encoded by *mew)* is particularly enriched in ISCs and critical for ISC maintenance (Lin et al., 2013), we sought to examine the role of the integrin αPS1and the critical integrin-interacting protein Talin in *esg^{ts}>yki^{3SA}* tumors, despite αPS1 not being identified in the tumor proteome (Fig. 3B). Thus, we examined the binding of Sd to the upstream regulatory region of *mew*, and given that TONDU peptide binds to Sd (Fig. 2D), we further reasoned that chromatin immunoprecipitation (ChIP)—using anti-FLAG antibody—on gut lysate of *esg^{ts}>yki^{3SA}* flies fed on FLAG-tagged TONDU peptide could reveal binding

of Sd. Indeed, we observed a significant enrichment of Sd binding in the upstream regulatory region of *mew, in vivo* in the guts of flies fed on FLAG-tagged TONDU peptide (47.04 ±2.3 %), as compared to unfed control (19.8±3.0%) (Fig. 3F), suggesting that TONDU peptide binds to Sd and therefore could interfere with transcriptional regulation of *mew* by the Yki-Sd complex in $esg^{ts}>yki^{3SA}$ tumors *in vivo*. By extension, it is likely that the TONDU peptide can also affect the expression of other transcriptional targets of Sd-Yki (Tables S2, S6) including other members of the integrin pathway.

Next, to assess the impact of TONDU peptide on the tumor proteome, we compared the proteome of $esg^{ts}>yki^{3SA}$ tumors with the proteome of $esg^{ts}>yki^{3SA}UAS\text{-}vg^{TONDU}$ and tumors from flies fed on 200 µM of the peptide. Our earlier observation of comparable phenotypic suppression of $esg^{ts}>yki^{3SA}$ tumors by either overexpression of TONDU peptide or its oral uptake, was supported by a strong correlation between their proteomes (Fig. S4B, C). Thus, we combined these two datasets for a robust representation of TONDU peptide-treated tumor proteome and compared it with that of untreated $esg^{ts}>yki^{3SA}$ tumors. We observed an overall decrease in levels of proteins in peptide-treated ISC tumors compared to those of $esg^{ts}>yki^{3SA}$ tumors from unfed controls (Fig. 3G). In addition, we noted that peptide-treated tumors displayed a significant decrease in protein levels (Fig. 3H) including that of critical members of the integrin pathway, such as Paxillin (-1.9 fold), Vinculin (-1.3 fold) and Talin (-1.2 fold) (Table S7).

Other notable perturbations included proteins involved in RNA processing, such as, Pre-RNA processing factor 19 (Prp19) (-2.16 fold) (Guilgur et al., 2014) and Rumpelstiltskin (Rump) (-3.15 fold). Furthermore, decrease in Chromosome bows (Chb) (-2.16 fold) which is involved in mitotic spindle assembly (Reis et al., 2009), could presumably contribute to the lowering of cell proliferation of peptide-treated tumors. We also noted a decrease (-2.3 fold) in mitochondrial trifunctional protein β (Mtp-β), which catalyzes oxidation of long chain fatty acids (Biswas et al., 2012), and could limit the energy source for peptide-treated tumors (Koundouros and Poulogiannis, 2020). Interestingly the tumor proteome revealed some novel and yet uncharacterized candidates that could be of functional significance. For instance, we noted a significant decrease in levels of proteins encoded by genes CG15784 (-2.65 fold) and CG7546 (-1.96 fold) in ISC tumors upon peptide treatment. Interestingly, these uncharacterized proteins interact with members of the Insulin/Akt (Vinayagam et al., 2016) and Hippo (Kwon et al., 2013) pathways, respectively, and could thus represent novel nodes connecting the Yki-oncogenic network with metabolic networks in the ISCs.

Taken together, our proteomic analyses reveal that TONDU peptide treatment perturbs a host of Yki-Sd targets that impinge upon cellular processes such as growth, proliferation and survival of tumor cells. It is likely that inhibition of *esg^{ts}>yki^{3SA}* tumors by the TONDU peptide could be a cumulative effect of suppression of multiple Yki-Sd targets affecting more than one signaling pathway or cellular process. We chose, however, to further examine the role of integrin signaling pathway since it plays a critical role in ISC maintenance (Lin et al., 2013).

Genetic suppression of integrin signaling phenocopies TONDU-mediated suppression of Yki-driven ISC tumors

Integrins form an essential component of the *Drosophila* gut epithelia, including the basally located ISCs (Lin et al., 2013; Chen et al., 2018). Integrin, such as αPS1is found specifically enriched in the ISCs (Lin et al., 2013) (also see Fig. 4A, B) and have been proposed to be important in the anchorage of the ISCs to the basement membrane and in their proliferation (Lin et al., 2013). Consistent with the enrichment of integrin pathway members in the *esg^{ts}>yki^{3SA}* proteome, we observed an overall increase in levels of integrin αPS1 (Fig. 4C) and Talin (Fig. 4D) in *esg^{ts}>yki^{3SA}* tumors. This observation, together with suppression of integrin pathway members such as Talin in TONDU peptide-fed flies suggests that integrin down-regulation is likely to be causally linked to TONDU peptide-mediated inhibition of *esg^{ts}>yki^{3SA}* tumors. To test this possibility, we down-regulated *rhea* or *mew* in the ISCs of *esg^{ts}>yki^{3SA}* tumors (Fig. 4E-G); indeed downregulation of *rhea (esg^{ts}>yki^{3SA}UAS-rhea-RNAi*, Fig. 4G) or *mew (esg^{ts}>yki^{3SA}UAS-mew-RNAi* Fig. 4F*)* resulted in a marked reduction in ISC numbers (Fig. 4H), which was most obvious in the anterior midgut (Fig. 4F and G) when compared to similarly aged *esg^{ts}>yki^{3SA}* tumors (Figs. 4E, S5A). Moreover, examination of early (day 3) *esg^{ts}>yki^{3SA}UAS-mew-RNAi* guts revealed poor growth of ISC tumors. In particular, most of the ISC tumors were made up of small cluster of 3 to 4 cells (Fig. S5 B, C), suggesting a strong decrease in tumor growth. These results are consistent with the observation that integrin signaling is required for ISC homeostasis (Lin et al., 2013). Interestingly, we note that gain of integrin alone, using a constitutively active form of the βPS integrin (Martin-Bermudo et al., 1999) in the ISCs (*esg^{ts}>torso$^{D/\beta Cyt}$*) failed to trigger ISC proliferation (Fig. S5D). These observations suggest that while gain of integrin signaling

alone *per se* does not transform ISCs, it is an essential partner for the progression of Yki-driven ISC tumors.

Discussion

Transcription factors (TFs) can be potent cancer drivers: suppression of TFs therefore constitutes a tumor inhibitory mechanism. The promise of targeting TFs for tumor therapy (Bhagwat and Vakoc, 2015; Lambert et al., 2018) is limited by the fact that small molecules often fail to target the large interacting surfaces associated with TFs (Lau and Dunn, 2018). Peptides, by contrast, have proven to be effective at interacting with large surfaces. Nevertheless, although peptides targeting extracellular receptors (Arosio et al., 2017) or intracellular inhibitors (Chang et al., 2013) have been explored, targeting of nuclear bound TFs with peptides remains poorly explored. The TEA/ATTS domain-containing TEAD proteins are a class of TFs that regulate YAP-induced proliferation and drive differentiation programs of VGLLs on the other (Gibault et al., 2018; Huh et al., 2019). In this study, using Yki-driven ISC tumors, we document *in vivo* inhibition of Yki-driven ISC tumor progression (Fig. 4I) by oral uptake of a *Drosophila* Vg-derived TONDU peptide. Remarkably, we observe a marked decrease in tumor load in TONDU peptide-fed flies, similar to what is observed upon ectopic expression of the peptide. Furthermore, a comparative proteomic analysis of ISC tumors in control and TONDU peptide-fed flies suggested a potential causal association between tumor suppression and down-regulation of the integrin signaling pathway, a key player implicated in ISC homeostasis (Lin et al., 2013). While our study strongly suggests a critical role of integrin pathway in Yki-driven tumorigenesis, however, a mechanistic understanding of how these regulate each other in ISC tumorigenesis remains to be further elucidated.

TONDU peptide derived from VGLL4 was earlier shown to inhibit gastric tumors in mouse xenograft models (Jiao et al., 2014). Here, we further show the ability of TONDU peptide to inhibit proliferation of prostate and colon cancer cell lines with elevated YAP1 levels. It is likely that other solid tumors with activated YAP/TAZ (Zanconato et al., 2016) and/or TEAD proteins (Gibault et al., 2018; Huh et al., 2019) could be sensitive to inhibition by the TONDU peptide. Moreover, tumors that display loss of tumor suppressor VGLLs (Deng and Fang, 2018), and thereby activated TEAD protein, are likely targets of TONDU peptide-mediated inhibition. Further, our finding that inhibition of integrins suppress Yki-driven tumors offers integrins as an alternate therapeutic target which being cell-membrane

localized could be readily accessed (Ley et al., 2016). Finally, cross-species conservation of integrin signaling pathways (Cooper and Giancotti, 2019) and YAP/TAZ activity (Sebe-Pedros et al., 2012) makes *Drosophila* tumor models ideal for exploring peptide and combinatorial therapeutic strategies for YAP-driven cancers.

It is noteworthy that peptide therapy in *Drosophila* has been successfully used to test therapeutic peptides that inhibit aggregate formation such as in Huntington's disease (Kazantsev et al., 2002) and Alzheimer's disease (Popiel et al., 2007) as well as peptides that exhibit immuno-modulatory roles (Pal et al., 2007). In most of these studies, however, peptides were injected into adult flies rather than administered orally. By contrast, oral administration of therapeutic peptides for treatment of human diseases, in general, carries the advantages of ease of administration, high patient compliance and often low production costs (Renukuntla et al., 2013). As is true for the development of small-molecule therapeutics, an *in vivo Drosophila* platform offers multiple advantages for peptide therapeutics, including: scalability, genetic tractability and rapid elucidation of the mechanistic underpinning of peptide-based tumor suppression. *Drosophila* has emerged as a powerful model system to design and screen novel small-molecule drugs (Dar et al., 2012; Markstein et al., 2014; Bangi et al., 2016) as potential treatments for diverse diseases, including cancers. Our study expands the repertoire of *Drosophila* model-based screening options to include peptides.

Extrapolation of the TONDU peptide as a therapeutic for intestinal cancer is not without caveats. In mammals, intestinal cancers arise from multiple cell types: intestinal crypt stem cells (Barker et al., 2009), crypt progenitors or transit amplifying cells and, occasionally, via reprogramming of differentiated intestinal cells (Sadanandam et al., 2013). In a subset ($Lgr5^{+}$) of crypt stem cells, gain of YAP surprisingly displays a tumor inhibitory role via its cytoplasmic sequestration of Disheveled (DVL) (Barry et al., 2013) or by inhibiting the activity of the TCF transcriptional complex (Li et al., 2020). However, in intestinal crypt cells, activation of YAP drives their unrestricted proliferation (Camargo et al., 2007; Zhou et al., 2011; Li et al., 2020) resulting in intestinal adenomas; this pro-tumorigenic property of YAP is TEAD dependent (Li et al., 2020). Given the dual role of YAP—tumor suppression versus tumor promotion—in a cell type-specific manner, TONDU peptide-mediated therapeutic strategy may hold promise only in intestinal cancers that are mediated by the pro-tumorigenic YAP-TEAD complex. Indeed, a number of inhibitors targeting YAP/TAZ-TEAD complexes have now shown therapeutic promises in arresting growth of cancers,

particularly those that display TEAD dependencies (for review, see (Pobbati and Hong, 2020).

Caveats and future directions

A major drawback of peptide therapeutics is the short half-life and poor bioavailability of the peptides. Use of non-natural amino acids (Verdurmen et al., 2011) and chemical modifications to stabilize the peptide backbone could help overcome these disadvantages (Furet et al., 2019). Moreover, oral administration of peptides presents additional challenges, including a need to survive harsh digestive milieu of the gastro-intestinal tract and their enzymatic degradation (Renukuntla et al., 2013). Furthermore, the intestinal mucosa is found to act as a barrier to peptide absorption. Indeed addition of TAT-domains that facilitate cellular uptake (Wang et al., 2017) to the TONDU peptide in our study could have contributed to the success of the oral TONDU peptide. Further improvement to stabilize therapeutic peptide to enhance bioavailability is a challenge for future work.

An additional challenge is that TFs can have multiple binding partners, such that targeting of a TF might result in off-target activities. For instance, with regard to the TONDU peptide, whereas *Drosophila* has a single TEAD protein, mammals have multiple TEAD proteins (TEAD1-4) that share the TONDU-interacting TEA/ATTS motif (Holden and Cunningham, 2018). This could lead to possible off-target activity of the TONDU peptide and consequent side effects. Further, since TEAD4 also binds to co-factors other than YAP and VGLLs such as the p160 nuclear receptors (Belandia and Parker, 2000), TONDU peptide administration might disrupt regulation by p160 of target genes which include chromatic modifiers and epigenetic regulators. Identifying and limiting off-target activity of TONDU peptide therefore presents future goals essential for its therapeutic use.

MATERIALS AND METHODS

MATERIALS

FLY LINES

	Fly Genotype	Source	
1	*UAS-yki$^{S111A.S168A.S250A}$*	#BDSC	#28817
2	*UAS-mew RNAi*	#BDSC	#27543
3	*UAS-rhea RNAi*	#BDSC	#28950
4	*esg-Gal4*	Norbert Perrimon, Harvard Medical School, USA	-
5	*UAS–torso^{D}/βcyt*	Nick Brown, University of Cambridge, UK	-

#Bloomington Drosophila Stock Center, Indiana University, Bloomington.

ANTIBODIES

	Protein	Catalog Number	Source	Raised in	Working dilution
1	Delta (extra cellular domain)	C594.9B	#DSHB	mouse	1:50
2	Sd	-	Gift from (De Celis lab)	rabbit	1:100
3	Talin (carboxy terminus 534 amino acids)	A22A	#DSHB	mouse	1:100
4	αPS1 (*mew*)	DK.1A4	#DSHB	mouse	1:50

#Developmental Studies Hybridoma Bank, University of Iowa.

PRIMER SEQUENCES

		Forward primer	Reverse primer
	For expression analysis		
1.	*ImpL2*	AAGAGCCGTGGACCTGGTA	TTGGTGAACTTGAGCCAGTCG
2.	*yki*	CCTTGCCGCCGGGATGG	TTTGCTGCTGCTGGCGATATTG
3	*delta*	AGCGACTCTTGGTGCAGCAGGTACT	TCCGTAGTAGTTGAGATCGCAGGTGAC
4	*myc*	ACACGCGCTGCAACGATATGG	CGAGGGATTTGTGGGTAGCTTCTT
5	*wg*	TGATGGCCCTGTGCAGCG	TGATGGCCCTGTGCAGCG
6	*ex*	GCCGCCTTTACCTGTCCAAC	CGTTCCGGTTTCCAATTAGCT
7	*β-tub*	CAAGCTGGCAGTGCGGCAAC	GCTGTCACCGTGGTAGGCGCC
8	*YAP1*	ACGTTCATCTGGGACAGCAT	GTTGGGAGATGGCAAAGACA
	ChIP PCR		
9	*Mew*	GCTTTGGTGGGGCTTGTAAC	GTAAAGGCATGAGCGCCAAAT

Genotype of the flies used in the study

1. Control flies bearing GFP-marked ISCs. (figures 1 and 4)
   esg-Gal4, tub-Gal80^{ts}, UAS-GFP; +
2. Gain of Yki (*UAS-yki$^{S111A.S168A.S250A}$* referred to as *UAS-Yki^{3SA}*) in ISCs. (figures 1, 2 and 4; figures S1 and S3)

esg-Gal4, tub-Gal80^{ts}, UAS-GFP/+; UAS-Yki^{3SA}/+

3. Simultaneous constitutively active Yki (*UAS-Yki^{3SA}*) and TONDU peptide in ISCs. (figure 2; figure S2)
   esg-Gal4, tub-Gal80^{ts}, UAS-GFP/+; UAS-Yki^{3SA}/+UAS-vg^{TONDU}/+
4. Downregulation of *mew* in ISCs expressing constitutively active Yki (figure 4)
   esg-Gal4, tub-Gal80^{ts}, UAS-GFP/+; UAS-Yki^{3SA}/+ UAS-mew RNAi/+
5. Downregulation of *rhea* in ISCs expressing a constitutively active Yki (figure S5)
   esg-Gal4, tub-Gal80^{ts}, UAS-GFP/+; UAS-Yki^{3SA}/+UAS-rhea RNAi/+
6. Constitutively active βintegrin in ISCs. (figure S5)
   esg-Gal4, tub-Gal80^{ts}, UAS-GFP/+; UAS–torso^{D}/βcyt

METHODS

Induction of Yki-driven ISC tumors.

We used the UAS-Gal4 system (Brand and Perrimon, 1993) to drive constitutively active Yki (*UAS-yki$^{S111A.S168A.S250A}$*) in which 3 Serine phosphorylation sites are mutated (Oh and Irvine, 2009; Kwon et al., 2015), in the intestinal stem cells (ISCs), using an ISC-specific Gal4 driver (*esg-Gal4*) under control of temperature sensitive tub-Gal80^{ts} (Kwon et al., 2015). Flies were mated and maintained at 18^{0}C until eclosion of the F1 generation. Freshly eclosed F1 flies of the genotype *esg>Gal4, tub-Gal80^{ts}UAS-yki^{3SA}* were shifted to 29^{0}C and maintained until dissection.

Generation of *UAS-vg^{TONDU}* fly line

We synthesized an oligonucleotide coding for the *Drosophila* TONDU domain (CVVFTNYSGDTASQVDEHFSRALNY) (Pobbati and Hong, 2013). We introduced a start (ATG) and stop codon (TAA) flanking the nucleotide sequences, and inserted a 5'EcoR1 and 3' Xba1 endonuclease restriction enzyme site on either side to allow directional cloning into pUASt vector (Addgene). We replaced Cytosine on position one and Alanine on position 22 with Serine (SVVFTNYSGDTASQVDEHFSRSLNY) to make the encoded peptide more polar and therefore improve its solubility. Substitution of terminal Cysteine would also reduce chances of aberrant dimer formation. The VXXHF domain of the TONDU domain,

which is essential for interaction with TEAD/Sd (Pobbati et al., 2012), was left unchanged. The synthesized oligo was cloned into pUAST vector carrying *mini white*, and injected into Canton S embryos at C-CAMP (Center for Cellular and Molecular Platforms, NCBS, Bangalore, India). Adults were screened for insertion of the vector into the third chromosome.

Design and synthesis of the TONDU peptide and its variants.

TONDU-peptide: We synthesized a peptide corresponding to the TONDU domain with certain modifications. The basic peptide is a 46 amino acid peptide (YGRKKRRQRRRGGPKKKRKVGG [VVFTNYSGDTASQVDEHFSRALNY]) comprised of 24 aa of the TONDU domain (VVFTNYSGDTASQVDEHFSRALNY) preceded by the conserved SV40 T-Antigen nuclear localizing signal (PKKKRKV) (Lanford et al., 1986) and a cell penetrating peptide (YGRKKRRQRRR) derived from human immunodeficiency virus (HIV) (Vives et al., 1997), the NLS sequence was flanked by a di-glycine (GG) spacer to avoid any steric hindrance between the tag and the rest of the peptide. The first Cytosine on the TONDU domain was removed to prevent dimerization of the peptide.

FLAG-tagged TONDU peptide: To test for binding partners to TONDU peptide, we added a FLAG tag (DYKDDDDK) at its C-terminus (YGRKKRRQRRRGGPKKKRKVGG-VVFTNYSGDTASQVDEHFSRALNYDYKDDDDK) to allow protein immunoprecipitation using an anti-FLAG antibody.

Fluorescent-tagged TONDU peptide: To track uptake of the peptide and facilitate its cellular localization, we added 5-TAMARA, a fluorescent tag, to the C-terminus of the TAT-NLS-TONDU peptide. The peptides were synthesized at GL Biochem Shanghai Ltd.

Administration of TONDU peptide: Lyophylized TONDU peptide was dissolved in water to a final concentration of 1 mM (used as stock), which was then used to prepare 50, 100, 200 or 400 µM of working stock. 100 µL of each was then sprayed over freshly cooled standard fly food (not containing any anti-fungal or anti-bacterial agent), on which flies were reared. The flies were transferred into fresh vials (containing TONDU peptide) every 24 hours for 10 days.

Immunostaining of *Drosophila* adult midguts

Prior to dissection, female flies of desired genotype were starved briefly and fed water for 2 hours to flush out food from the gut. Midguts were dissected in 1X PBS and fixed in 4% paraformaldehyde in PBS containing 0.2% triton X-100 for 30 minutes at room temperature; followed by washing in PBS containing 0.2% triton X-100 for 15 minutes. The guts were then incubated in primary antibody at 4^0C overnight, followed by blocking with 0.1 % BSA for 1 hour and incubation with secondary antibody (Alexa fluor 555 against mouse or rabbit) for 4 hours at room temperature. Next, guts were washed in 1X PBS and counterstained for nuclei using TOPRO (Invitrogen, S33025) or F-actin using Alexa Fluor Phalloidin-633 (Invitrogen A22284, 1:100), followed by mounting in an anti-fade mounting medium, Vectashield (Sigma).

Microscopy and Image Processing

Images were acquired using a Leica SP5 confocal microscope and processed using the Leica application software and Adobe Photoshop CS5.

Measurement of GFP from confocal images.

GFP was quantitated from full projections of images acquired using confocal microscopy. GFP intensity in gray scale from ROIs covering the entire gut was acquired using the Leica-LSM proprietary software. GFP intensity was normalized to the area of each ROI. Student t-test was done using MS-Excel to look for statistical significance in GFP variation.

EdU cell proliferation assay

Cell proliferation was detected by EdU uptake using Click-iT Alexa-Fluor-555 290 kit by Invitrogen. Briefly, unfixed guts from female *esg^{ts}>UAS-yki^{3SA}*flies were incubated with 100 µM of EdU in Schneider's insect medium, for one hour at room temperature. Tissue was then fixed in 4% paraformaldehyde and incubated in secondary buffer containing fluorescent-tagged dye (following manufacturer's instruction) for one hour at room temperature and subsequently washed in PBS, counter-stained with TO-PRO-3 (Invitrogen, S33025) and mounted using an anti-fade mounting medium (Invitrogen).

Quantitative RT-PCR

RT-PCR was performed using SYBR green (Applied Biosystems) on ABI7 900 HT. Prior to dissection, *esg^{ts}>UAS-yki^{3SA}* females were starved briefly and fed water for 2 hours to flush out food from the gut. Total RNA from 20 midguts was isolated using QiagenRNeasy columns. RNA was treated with RNase-free DNase (Roche) to get rid of any traces of DNA before converting RNA to cDNA using a cDNA preparation kit (Invitrogen). The resulting cDNA was used as substrate for relative quantitation using SYBR green on ABI7 900 HT. β-Tubulin was used as an endogenous control. Genes were assayed from four biological replicates for each condition. qPCR was performed using the following conditions: DNA polymerase activation for 10 min at 95°C, followed by 40 cycles of duplex melting for 15 s at 95°C and a combined annealing and extension step for 1 min at 60°C. The threshold-cycle (Ct) values were generated automatically. The relative expression value of each gene in the two conditions was calculated using the 2-ΔΔCt method.

Cancer cell line and cell culture conditions

The prostate (PC3 and LNCaP) and colorectal (Colo 320-HSR) cancer cell lines were obtained from American Type Cell Culture (ATCC, Manassas, VA, USA). The colorectal cancer cell line WiDr was a kind gift from Dr. Eric R. Fearon, University of Michigan, Ann Arbor, MI, USA. All of the cell lines were cultured as per ATCC guidelines in a CO_2 incubator (Thermo-Fisher) supplied with 5% CO_2 at 37°C temperature. Cell line authentication was done via short tandem repeats (STR) profiling at Lifecode Technologies Private Limited (Bangalore, India) and DNA Forensics Laboratory (New Delhi, India). Routine check for mycoplasma contamination of all cell lines was carried out using PlasmoTest mycoplasma detection kit (InvivoGen).

Cell viability assay of human cancer cell lines

To determine the effect of TONDU peptides on the cell viability of prostate cancer (PC3 and LNCaP) and colorectal cancer (COLO320 and WiDR) cells. Approximately 3,000 cells were plated in each well of a 96-well plate. After 24 hours, TONDU peptide was added to the cultured cells at three different concentrations: 50 nM, 100 nM and 250 nM. No peptide was

added in the control group. After 72 and 96 hours of peptide treatment, cell viability was determined using resazurin sodium salt solution (R7107, Sigma). Briefly, resazurin (0.02mg/ml; w/v) diluted in culture media was added to the cells and incubated for 4 hours in the dark at 37ºC. The fluorescence was measured at 530/590 nm (excitation/emission) using BioTek™ Synergy™ H4 Hybrid Microplate Reader (Winooski, VT, USA).

Statistical significance

Biologically independent samples were used (n=3) in each experiment; data represents mean ± SEM. Statistical significance was determined using two-tailed unpaired Student's t-test, and ∗P≤ *0.001*.

Immunoprecipitation studies to determine binding of TONDU peptide to Sd

- ***Drosophila* cell line**

  Drosophila S2R+ cells (sex: male) were cultured in Schneider's medium supplemented with 10% fetal bovine serum (FBS) at 25°C.

- **Plasmids used for immunoprecipitation studies**

  Full-length Sd (GEO03367) and Yki (GEO02945) cDNAs from the Drosophila Genomics Resource Center were cloned into the Drosophila Gateway vector pAWH and pAWG respectively. GFP was cloned into pAWM as a control.

- **Immunoprecipitation and Immunoblotting**

  Immunoprecipitation and Immunoblotting were performed as previously described (Tang et al., 2018). In brief, DNA was transfected into S2R+ using Effectene transfection reagent (Qiagen, 301427). After 2 days of incubation, cells were incubated with or without 1 µM TONDU peptide for 24 hrs and then lysed with lysis buffer (Pierce 87788) containing a protease and phosphatase inhibitor cocktail (Pierce, 78440). Lysate was incubated with Chromotek-GFP-Trap (Bulldog Biotechnology, gta-20) for 2 hrs at 4°C to precipitate the proteins. Beads were washed 3-4 times with 1 mL lysis buffer and then boiled in SDS sample buffer, run on a 4%–20% polyacrylamide gel (Bio-Rad, 4561096), and transferred to an Immobilon-P polyvinylidene fluoride (PVDF) membrane (Millipore). The membrane was blocked by 5% BSA in TBST (TBS with 0.1% Tween-20) in room temperature for 1 hour and then probed with anti-GFP (Molecular Probes, A6455), anti-HA (Covance/BioLegend, MMS-101P), or anti-FLAG (Sigma, F3165) antibody in 1X TBST with 5% BSA overnight, followed by HRP-conjugated secondary antibody, and

signal was detected by enhanced chemiluminescence (ECL; Amersham, RPN2209; Pierce, 34095).

- For the TONDU-Sd binding assay, HA-Sd was expressed in S2R+ cells and purified through immunoprecipitation with RIPA buffer (Pierce, 89901) and anti-HA agarose (Sigma, A2095). Purified HA-Sd proteins were incubated with 1 µM TONDU peptide directly. The sample was then washed and subjected to immunoblotting.

Quantitation of the effect of the TONDU peptide on Yki-Sd-driven transcription using HRE

Luciferase reporter

Drosophila S2R+ cells were maintained at 25^0C in Schneider's medium (GIBCO) with 10% heat-inactivated fetal bovine serum (Sigma) and 5% Pen-Strep (GIBCO). Experiments were run in 24-well plate, three replicates per condition. Cells were co-transfected with 100 ng each of 1) HRE-luciferase reporter (containing two copies of a Hippo Response Element cloned upstream of a hsp70 basal promoter in pGL3 basic vector (Wu et al., 2008)), along with 2) Sd- or 3) Yki-expressing pAc5.1/V5-HisB plasmids (Wu et al., 2008) (gift from D. Pan); 10 ng of Act-Renilla was used for transfection control. Transfection was carried out using Effectene (Qiagen), as per manufacturer's recommended protocol. 24 hours after transfection, 50 or 100 nM of the TONDU peptide was added to wells in triplicate. 48 hours after addition of the TONDU peptide, cells were harvested and Luciferase activity was measured using Dual Glo (Promega) as per the kit instructions, and measured using a Spectramax Luminescence plate reader.

Detection of fluorescent labeled TONDU peptide in S2R+ cells

Drosophila S2R+ cells were grown to confluence in Schneider's medium (GIBCO) supplemented with 10% heat-inactivated fetal bovine serum (Sigma), and 5% Pen-Strep (GIBCO) at 25^0C in 24 well plates. TAMARA-tagged TONDU peptide was added to the medium to a final concentration of 100 nM and cells were incubated for 6 hours. Next, the medium was discarded and cells washed 3 times with 1XPBS. Cells were then added to

lysine coated slides, fixed with 4% formaldehyde in 1XPBS, and counterstained with DAPI. Cells were imaged with a Nikon Ti, CSU-X1 spinning disk confocal microscope and the images were processed using Fiji image processing software (https://imagej.net › Fiji).

Chromatin immunoprecipitation (ChIP) to determine binding of TONDU peptide to Sd in the upstream regulatory region of gene *mew*

ChIP was performed using LowCell# ChIP kit protein A (Diagenode Cat# C01010072) according to manufacturer's instructions. Briefly, midguts from 35 adult *esg^{ts}>UAS-yki^{3SA}* females (pre-starved for 1 hour) were dissected in ice-cold 1XPBS and crosslinked in 1% formaldehyde (Sigma) for 15 minutes at 37^{0}C. Crosslinking was quenched with 125 mM Glycine. The guts were washed with PBS and precipitated with centrifugation at 6000 rpm for 5 minutes. The pellet was lysed in 250 mL of Buffer B (LowCell# ChIP kit) supplemented with complete protease inhibitor (Roche) and PMSF (Sigma). 130 µL of lysed chromatin was sheared using a Bioruptor (Diagenode) at high frequency for 15 cycles of 30 sec ON, 30 sec OFF. 870 µL of Buffer A (LowCell# ChIP kit) supplemented with complete protease inhibitor (Roche) and PMSF (Sigma) was added to the shared chromatin. 8 µL of the chromatin solution was saved as an input control. 11 µL of magnetic beads was washed twice with Buffer-A (LowCell# ChIP kit) and resuspended in 800 µL of Buffer A. 2 µg of Anti-FLAG antibody (Sigma, F1804) were added to the washed beads and gently agitated at 4^{0}C for 4 hours. The beads-antibody complex was precipitated with a magnet and the supernatant was removed. 800 µL of shared chromatin was added to the beads-antibody complex and rotated at 4^{0}C overnight. The immobilized chromatin was then washed with Buffer A three times and Buffer C once, and eluted in 100 µL elution buffer (1% SDS, 0.1 M sodium bicarbonate with proteinase K and RNaseA). The chromatin was subjected to either phenol-chloroform extraction for DNA purification and subsequent qPCR analysis; or the protein or the protein was extracted by heating the washed beads at 95^{0}C in 20 ul SDS loading dye (4X) for 10 minutes and centrifuged at 13000 rpm for 10 minutes. The supernatant was collected and used for dot blot analysis.

Protein dot blot

1 mM TONDU peptide was serially diluted (10^{-1}, 10^{-2}, 10^{-3}) and blotted using a narrow-mouth pipette tip, and 7.5 µl of peptide or enriched protein fraction from ChIP were applied

slowly onto the nitrocellulose membrane (Thermo Fisher, 0.2 um pore size). The membrane was air dried and then blocked in 5% BSA in TBS-T (Tris-buffered saline, 0.1% Tween 20) for 2 hours at RT, then incubated for 3 hours with a secondary antibody conjugated with HRP (Jackson ImmunoResearch #711035152), washed three times with TBST, and then detected with chemiluminescent substrate (Thermofischer#34080) and visualized on X-ray film (Fuji, Super HR-t).

Proteomics of Yki-driven ISC tumors

- **Protein extraction from fly guts for LC-MS-MS analysis**

Prior to dissection, female *esg^{ts}>UAS-yki^{3SA}* flies were briefly starved and fed on water for 2 hours to clear the gut. Adult guts were dissected in cold 1X PBS from 20 flies. The fore- and hindguts were removed, and the midguts were put in 100 µl extraction buffer (6M GnHCl in 50mM Tris-Cl pH 7.4, 65 mM DTT) with 50 mM sodium acetate and protease inhibitors (1X protease inhibitor cocktail with 0.2 mM PMSF) was added to the sample. The guts were sonicated with a Bioruptor (Diagenode) using the following settings: Sonication cycle: 30 sec ON and 30 sec OFF for 5 cycles at 4˚C. Cell debris were removed by brief centrifuging it at 8000 RPM for 3 minutes; then the supernatant was transferred to a new tube. The protein concentration was determined spectrophotometrically using Nanodrop and using BCA protein assay (Thermo fisher) following manufacturer's protocol. 5µg of the protein was used for LC-MS-MS analysis. We made certain that the tissue was processed within half an hour of dissection.

- **Sample preparation for LC-MS/MS**

5 µg of the protein samples were reduced with 5 mM TCEP, further alkylated with 50 mM iodoacetamide, and digested with Trypsin (1:50, Trypsin/lysate ratio) for 16 hours at 37°C. Digests were cleaned using a C18 silica cartridge to remove the salt and dried using a speed vac. The dried pellet was resuspended in 5% acetonitrile, 0.1% formic acid (Buffer A).

- **Mass Spectrometric Analysis of Peptide Mixtures**

The experiment was performed using an EASY-nLC 1000 system (Thermo Fisher Scientific) coupled to a Thermo Fisher-Orbitrap *Fusion* mass spectrometer equipped with a nanoelectrospray ion source. 1.0 µg of the peptide mixture was resolved using a 25 cm

Thermo Easy-spray PepMap C18 column. The peptides were loaded with Buffer A and eluted with a 0–40% gradient of Buffer B (95% acetonitrile, 0.1% formic acid) at a flow rate of 300 nL/min for 60 min. MS data was acquired using a data-dependent top 20 method dynamically choosing the most abundant precursor ions from the survey scan. The LC MS/MS .RAW files have been submitted to MassIVE repository (https://massive.ucsd.edu) and can be accessed using MSV000084841.

Data Processing

All samples were processed and the 8 RAW files generated were analyzed with Proteome Discoverer (v2.2) against the Uniprot *Drosophila melanogaster* reference proteome database. For Sequest search, the precursor and fragment mass tolerances were set at 10 ppm and 0.5 Da, respectively. The protease used to generate peptides, *i.e.* enzyme specificity, was set for trypsin/P (cleavage at the C terminus of "K/R: unless followed by "P") along with a maximum missed cleavages value of two. Carbamidomethyl on cysteine as fixed modification and oxidation of methionine and N-terminal acetylation were considered as variable modifications for database search. Both the peptide spectrum match and the protein false discovery rate were set to 0.01 FDR.

Proteome data analysis

To identify biologically relevant protein signatures in $esg^{ts}>yki^{3SA}$ tumors and characterize their status in the presence of the TONDU peptide, we calculated the log2 abundance ratios, using mean abundance values for individual Uniprot IDs of $esg^{ts}>UAS\text{-}yki^{3SA}$ day 7 versus day 1 proteome. Only those were taken into consideration whose combined FDR confidence was <0.05 (medium) or <0.01 (high), while those with >0.05 (low) were discarded. We further filtered out peptides that were not detected in either MS, or MS-MS spectrum, depending on its peak calling. We noted that the number of peptides that matched each Uniprot ID, ranged from 1 to 67. To ascertain statistically significant calls, we applied student t-test on replicate readings for the individual Uniprot IDs and only those with $P<0.05$ were considered. We first calculated $\log_2$ abundance ratio of proteins in day 7 with day 1 of $esg^{ts}>yki^{3SA}$ tumors, and considered only gene products whose log2 fold change was ≥ 2. Next, we examined the status of tumor proteins from TONDU peptide-fed flies. Since the TONDU-peptide treated tumors phenocopied the tumor suppression seen by overexpression

of the TONDU peptide (compare Fig. 1 with Fig. 2), and since their protein profiles displayed closed correlation (Fig S4), we chose to combine these two data sets. We therefore calculated $\log_2$ abundance ratio of individual proteins in untreated day 7 *esg*^{ts}>*yki*^{3SA} tumors, to that of TONDU peptide-treated and to TONDU-peptide expressed (*UAS-vg*^{TONDU}) ISC tumors. We applied the Student t-test to look for statistical significance for each log2 fold change, and considered only those with $P<0.05$.

Gene Ontology Analysis

To identify biological function of genes and look for enrichment of functional classes, we undertook Gene Ontology analysis using PANTHER (Protein ANalysisTHroughEvolutionaryRelationships) classification system (http://www.pantherdb.org, (Mi et al., 2007). Protein functions were inferred by classification of genes into one or more groups, depending on: 1) Molecular function, 2) Biological Process, 3) Protein class, 4) Pathways, and 5) Cellular component.

Heat Maps

Heat maps were generated using Heatmapper (http://heatmapper.ca/). For the heatmap in Fig 3A, raw abundance values for individual UniProt IDs were subjected to row scaling, and clustered using average linkage clustering with Euclidean method for distance measure.

DATA AVAILABILITY: The LC MS/MS reads for unlabeled proteomics generated in this study is available at to MassIVE repository (https://massive.ucsd.edu) and can be accessed using MSV000084841.

ACKNOWLEDGEMENTS

We thank Jose F. de Celis for the antibody against Sd, Duojia Pan for HRE-Luciferase reporter vectors, Nick Brown for the UAS-*torso*$^{D/\beta Cyt}$ fly line, and Stephanie Mohr for comments on the manuscript. We also acknowledge the fly transgenic facility at C-CAMP (Center for Cellular and Molecular Platforms, NCBS, Bangalore, India) and proteomics service by Valerian Chem, Gurgaon, India. This study was supported by the DBT/Wellcome Trust India
Alliance -Early Career Fellowship (IA/E/13/1/501271) to AB.

COMPETING INTEREST: The authors declare no competing interest.

REFERENCE

Arosio, D., Manzoni, L., Corno, C. and Perego, P. (2017) 'Integrin-Targeted Peptide- and Peptidomimetic-Drug Conjugates for the Treatment of Tumors', *Recent Pat Anticancer Drug Discov* 12(2): 148-168.

Bajpai, A. and Sinha, P. (2020) 'Hh signaling from de novo organizers drive lgl neoplasia in Drosophila epithelium', *Dev Biol* 457(1): 1-8.

Bangi, E., Murgia, C., Teague, A. G., Sansom, O. J. and Cagan, R. L. (2016) 'Functional exploration of colorectal cancer genomes using Drosophila', *Nat Commun* 7: 13615.

Bantscheff, M., Schirle, M., Sweetman, G., Rick, J. and Kuster, B. (2007) 'Quantitative mass spectrometry in proteomics: a critical review', *Anal Bioanal Chem* 389(4): 1017-31.

Barker, N., Ridgway, R. A., van Es, J. H., van de Wetering, M., Begthel, H., van den Born, M., Danenberg, E., Clarke, A. R., Sansom, O. J. and Clevers, H. (2009) 'Crypt stem cells as the cells-of-origin of intestinal cancer', *Nature* 457(7229): 608-11.

Barry, E. R., Morikawa, T., Butler, B. L., Shrestha, K., de la Rosa, R., Yan, K. S., Fuchs, C. S., Magness, S. T., Smits, R., Ogino, S. et al. (2013) 'Restriction of intestinal stem cell expansion and the regenerative response by YAP', *Nature* 493(7430): 106-10.

Belandia, B. and Parker, M. G. (2000) 'Functional interaction between the p160 coactivator proteins and the transcriptional enhancer factor family of transcription factors', *J Biol Chem* 275(40): 30801-5.

Bhagwat, A. S. and Vakoc, C. R. (2015) 'Targeting Transcription Factors in Cancer', *Trends Cancer* 1(1): 53-65.

Biswas, S., Lunec, J. and Bartlett, K. (2012) 'Non-glucose metabolism in cancer cells--is it all in the fat?', *Cancer Metastasis Rev* 31(3-4): 689-98.

Brand, A. H. and Perrimon, N. (1993) 'Targeted gene expression as a means of altering cell fates and generating dominant phenotypes', *Development* 118(2): 401-15.

Camargo, F. D., Gokhale, S., Johnnidis, J. B., Fu, D., Bell, G. W., Jaenisch, R. and Brummelkamp, T. R. (2007) 'YAP1 increases organ size and expands undifferentiated progenitor cells', *Curr Biol* 17(23): 2054-60.

Chang, Y. S., Graves, B., Guerlavais, V., Tovar, C., Packman, K., To, K. H., Olson, K. A., Kesavan, K., Gangurde, P., Mukherjee, A. et al. (2013) 'Stapled alpha-helical peptide drug development: a potent dual inhibitor of MDM2 and MDMX for p53-dependent cancer therapy', *Proc Natl Acad Sci U S A* 110(36): E3445-54.

Chen, J., Sayadian, A. C., Lowe, N., Lovegrove, H. E. and St Johnston, D. (2018) 'An alternative mode of epithelial polarity in the Drosophila midgut', *PLoS Biol* 16(10): e3000041.

Cooper, J. and Giancotti, F. G. (2019) 'Integrin Signaling in Cancer: Mechanotransduction, Stemness, Epithelial Plasticity, and Therapeutic Resistance', *Cancer Cell* 35(3): 347-367.

Dar, A. C., Das, T. K., Shokat, K. M. and Cagan, R. L. (2012) 'Chemical genetic discovery of targets and anti-targets for cancer polypharmacology', *Nature* 486(7401): 80-4.

Deng, X. and Fang, L. (2018) 'VGLL4 is a transcriptional cofactor acting as a novel tumor suppressor via interacting with TEADs', *Am J Cancer Res* 8(6): 932-943.

Drucker, D. J. (2019) 'Advances in oral peptide therapeutics', *Nat Rev Drug Discov*.

Furet, P., Salem, B., Mesrouze, Y., Schmelzle, T., Lewis, I., Kallen, J. and Chene, P. (2019) 'Structure-based design of potent linear peptide inhibitors of the YAP-TEAD protein-protein interaction derived from the YAP omega-loop sequence', *Bioorg Med Chem Lett* 29(16): 2316-2319.

Gibault, F., Sturbaut, M., Bailly, F., Melnyk, P. and Cotelle, P. (2018) 'Targeting Transcriptional Enhanced Associate Domains (TEADs)', *J Med Chem* 61(12): 5057-5072.

Guilgur, L. G., Prudencio, P., Sobral, D., Liszekova, D., Rosa, A. and Martinho, R. G. (2014) 'Requirement for highly efficient pre-mRNA splicing during Drosophila early embryonic development', *Elife* 3: e02181.

Guo, T., Lu, Y., Li, P., Yin, M. X., Lv, D., Zhang, W., Wang, H., Zhou, Z., Ji, H., Zhao, Y. et al. (2013) 'A novel partner of Scalloped regulates Hippo signaling via antagonizing Scalloped-Yorkie activity', *Cell Res* 23(10): 1201-14.
Guo, Z., Lucchetta, E., Rafel, N. and Ohlstein, B. (2016) 'Maintenance of the adult Drosophila intestine: all roads lead to homeostasis', *Curr Opin Genet Dev* 40: 81-86.
Holden, J. K. and Cunningham, C. N. (2018) 'Targeting the Hippo Pathway and Cancer through the TEAD Family of Transcription Factors', *Cancers (Basel)* 10(3).
Huh, H. D., Kim, D. H., Jeong, H. S. and Park, H. W. (2019) 'Regulation of TEAD Transcription Factors in Cancer Biology', *Cells* 8(6).
Jiao, S., Wang, H., Shi, Z., Dong, A., Zhang, W., Song, X., He, F., Wang, Y., Zhang, Z., Wang, W. et al. (2014) 'A peptide mimicking VGLL4 function acts as a YAP antagonist therapy against gastric cancer', *Cancer Cell* 25(2): 166-80.
Jin, Y., Xu, J., Yin, M. X., Lu, Y., Hu, L., Li, P., Zhang, P., Yuan, Z., Ho, M. S., Ji, H. et al. (2013) 'Brahma is essential for Drosophila intestinal stem cell proliferation and regulated by Hippo signaling', *Elife* 2: e00999.
Kazantsev, A., Walker, H. A., Slepko, N., Bear, J. E., Preisinger, E., Steffan, J. S., Zhu, Y. Z., Gertler, F. B., Housman, D. E., Marsh, J. L. et al. (2002) 'A bivalent Huntingtin binding peptide suppresses polyglutamine aggregation and pathogenesis in Drosophila', *Nat Genet* 30(4): 367-76.
Khan, S. J., Bajpai, A., Alam, M. A., Gupta, R. P., Harsh, S., Pandey, R. K., Goel-Bhattacharya, S., Nigam, A., Mishra, A. and Sinha, P. (2013) 'Epithelial neoplasia in Drosophila entails switch to primitive cell states', *Proc Natl Acad Sci U S A* 110(24): E2163-72.
Khoo, P., Allan, K., Willoughby, L., Brumby, A. M. and Richardson, H. E. (2013) 'In Drosophila, RhoGEF2 cooperates with activated Ras in tumorigenesis through a pathway involving Rho1-Rok-Myosin-II and JNK signalling', *Dis Model Mech* 6(3): 661-78.
Koontz, L. M., Liu-Chittenden, Y., Yin, F., Zheng, Y., Yu, J., Huang, B., Chen, Q., Wu, S. and Pan, D. (2013) 'The Hippo effector Yorkie controls normal tissue growth by antagonizing scalloped-mediated default repression', *Dev Cell* 25(4): 388-401.
Koundouros, N. and Poulogiannis, G. (2020) 'Reprogramming of fatty acid metabolism in cancer', *Br J Cancer* 122(1): 4-22.
Kwon, Y., Song, W., Droujinine, I. A., Hu, Y., Asara, J. M. and Perrimon, N. (2015) 'Systemic organ wasting induced by localized expression of the secreted insulin/IGF antagonist ImpL2', *Dev Cell* 33(1): 36-46.
Kwon, Y., Vinayagam, A., Sun, X., Dephoure, N., Gygi, S. P., Hong, P. and Perrimon, N. (2013) 'The Hippo signaling pathway interactome', *Science* 342(6159): 737-40.
Lambert, M., Jambon, S., Depauw, S. and David-Cordonnier, M. H. (2018) 'Targeting Transcription Factors for Cancer Treatment', *Molecules* 23(6).
Lanford, R. E., Kanda, P. and Kennedy, R. C. (1986) 'Induction of nuclear transport with a synthetic peptide homologous to the SV40 T antigen transport signal', *Cell* 46(4): 575-82.
Lau, J. L. and Dunn, M. K. (2018) 'Therapeutic peptides: Historical perspectives, current development trends, and future directions', *Bioorg Med Chem* 26(10): 2700-2707.
Ley, K., Rivera-Nieves, J., Sandborn, W. J. and Shattil, S. (2016) 'Integrin-based therapeutics: biological basis, clinical use and new drugs', *Nat Rev Drug Discov* 15(3): 173-83.
Li, Q., Sun, Y., Jarugumilli, G. K., Liu, S., Dang, K., Cotton, J. L., Xiol, J., Chan, P. Y., DeRan, M., Ma, L. et al. (2020) 'Lats1/2 Sustain Intestinal Stem Cells and Wnt Activation through TEAD-Dependent and Independent Transcription', *Cell Stem Cell* 26(5): 675-692 e8.
Lin, G., Zhang, X., Ren, J., Pang, Z., Wang, C., Xu, N. and Xi, R. (2013) 'Integrin signaling is required for maintenance and proliferation of intestinal stem cells in Drosophila', *Dev Biol* 377(1): 177-87.
Markstein, M., Dettorre, S., Cho, J., Neumuller, R. A., Craig-Muller, S. and Perrimon, N. (2014) 'Systematic screen of chemotherapeutics in Drosophila stem cell tumors', *Proc Natl Acad Sci U S A* 111(12): 4530-5.

Martin-Bermudo, M. D., Alvarez-Garcia, I. and Brown, N. H. (1999) 'Migration of the Drosophila primordial midgut cells requires coordination of diverse PS integrin functions', *Development* 126(22): 5161-9.
Mi, H., Guo, N., Kejariwal, A. and Thomas, P. D. (2007) 'PANTHER version 6: protein sequence and function evolution data with expanded representation of biological pathways', *Nucleic Acids Res* 35(Database issue): D247-52.
Mulligan, K. A., Fuerer, C., Ching, W., Fish, M., Willert, K. and Nusse, R. (2012) 'Secreted Wingless-interacting molecule (Swim) promotes long-range signaling by maintaining Wingless solubility', *Proc Natl Acad Sci U S A* 109(2): 370-7.
Nagaraj, R., Gururaja-Rao, S., Jones, K. T., Slattery, M., Negre, N., Braas, D., Christofk, H., White, K. P., Mann, R. and Banerjee, U. (2012) 'Control of mitochondrial structure and function by the Yorkie/YAP oncogenic pathway', *Genes Dev* 26(18): 2027-37.
Oh, H. and Irvine, K. D. (2009) 'In vivo analysis of Yorkie phosphorylation sites', *Oncogene* 28(17): 1916-27.
Oh, H., Slattery, M., Ma, L., Crofts, A., White, K. P., Mann, R. S. and Irvine, K. D. (2013) 'Genome-wide association of Yorkie with chromatin and chromatin-remodeling complexes', *Cell Rep* 3(2): 309-18.
Pal, S., St Leger, R. J. and Wu, L. P. (2007) 'Fungal peptide Destruxin A plays a specific role in suppressing the innate immune response in Drosophila melanogaster', *J Biol Chem* 282(12): 8969-77.
Pobbati, A. V., Chan, S. W., Lee, I., Song, H. and Hong, W. (2012) 'Structural and functional similarity between the Vgll1-TEAD and the YAP-TEAD complexes', *Structure* 20(7): 1135-40.
Pobbati, A. V. and Hong, W. (2013) 'Emerging roles of TEAD transcription factors and its coactivators in cancers', *Cancer Biol Ther* 14(5): 390-8.
Pobbati, A. V. and Hong, W. (2020) 'A combat with the YAP/TAZ-TEAD oncoproteins for cancer therapy', *Theranostics* 10(8): 3622-3635.
Popiel, H. A., Nagai, Y., Fujikake, N. and Toda, T. (2007) 'Protein transduction domain-mediated delivery of QBP1 suppresses polyglutamine-induced neurodegeneration in vivo', *Mol Ther* 15(2): 303-9.
Reis, R., Feijao, T., Gouveia, S., Pereira, A. J., Matos, I., Sampaio, P., Maiato, H. and Sunkel, C. E. (2009) 'Dynein and mast/orbit/CLASP have antagonistic roles in regulating kinetochore-microtubule plus-end dynamics', *J Cell Sci* 122(Pt 14): 2543-53.
Renukuntla, J., Vadlapudi, A. D., Patel, A., Boddu, S. H. and Mitra, A. K. (2013) 'Approaches for enhancing oral bioavailability of peptides and proteins', *Int J Pharm* 447(1-2): 75-93.
Sadanandam, A., Lyssiotis, C. A., Homicsko, K., Collisson, E. A., Gibb, W. J., Wullschleger, S., Ostos, L. C., Lannon, W. A., Grotzinger, C., Del Rio, M. et al. (2013) 'A colorectal cancer classification system that associates cellular phenotype and responses to therapy', *Nat Med* 19(5): 619-25.
Sebe-Pedros, A., Zheng, Y., Ruiz-Trillo, I. and Pan, D. (2012) 'Premetazoan origin of the hippo signaling pathway', *Cell Rep* 1(1): 13-20.
Song, W., Kir, S., Hong, S., Hu, Y., Wang, X., Binari, R., Tang, H. W., Chung, V., Banks, A. S., Spiegelman, B. et al. (2019) 'Tumor-Derived Ligands Trigger Tumor Growth and Host Wasting via Differential MEK Activation', *Dev Cell* 48(2): 277-286 e6.
Szklarczyk, D., Gable, A. L., Lyon, D., Junge, A., Wyder, S., Huerta-Cepas, J., Simonovic, M., Doncheva, N. T., Morris, J. H., Bork, P. et al. (2019) 'STRING v11: protein-protein association networks with increased coverage, supporting functional discovery in genome-wide experimental datasets', *Nucleic Acids Res* 47(D1): D607-D613.
Tang, H. W., Hu, Y., Chen, C. L., Xia, B., Zirin, J., Yuan, M., Asara, J. M., Rabinow, L. and Perrimon, N. (2018) 'The TORC1-Regulated CPA Complex Rewires an RNA Processing Network to Drive Autophagy and Metabolic Reprogramming', *Cell Metab* 27(5): 1040-1054 e8.
Verdurmen, W. P., Bovee-Geurts, P. H., Wadhwani, P., Ulrich, A. S., Hallbrink, M., van Kuppevelt, T. H. and Brock, R. (2011) 'Preferential uptake of L- versus D-amino acid cell-penetrating peptides in a cell type-dependent manner', *Chem Biol* 18(8): 1000-10.

Vinayagam, A., Kulkarni, M. M., Sopko, R., Sun, X., Hu, Y., Nand, A., Villalta, C., Moghimi, A., Yang, X., Mohr, S. E. et al. (2016) 'An Integrative Analysis of the InR/PI3K/Akt Network Identifies the Dynamic Response to Insulin Signaling', *Cell Rep* 16(11): 3062-3074.
Vives, E., Brodin, P. and Lebleu, B. (1997) 'A truncated HIV-1 Tat protein basic domain rapidly translocates through the plasma membrane and accumulates in the cell nucleus', *J Biol Chem* 272(25): 16010-7.
Wadia, J. S. and Dowdy, S. F. (2005) 'Transmembrane delivery of protein and peptide drugs by TAT-mediated transduction in the treatment of cancer', *Adv Drug Deliv Rev* 57(4): 579-96.
Wang, X., Qiao, Y., Asangani, I. A., Ateeq, B., Poliakov, A., Cieslik, M., Pitchiaya, S., Chakravarthi, B., Cao, X., Jing, X. et al. (2017) 'Development of Peptidomimetic Inhibitors of the ERG Gene Fusion Product in Prostate Cancer', *Cancer Cell* 31(4): 532-548 e7.
Wu, S., Liu, Y., Zheng, Y., Dong, J. and Pan, D. (2008) 'The TEAD/TEF family protein Scalloped mediates transcriptional output of the Hippo growth-regulatory pathway', *Dev Cell* 14(3): 388-98.
Zanconato, F., Cordenonsi, M. and Piccolo, S. (2016) 'YAP/TAZ at the Roots of Cancer', *Cancer Cell* 29(6): 783-803.
Zhang, W., Gao, Y., Li, P., Shi, Z., Guo, T., Li, F., Han, X., Feng, Y., Zheng, C., Wang, Z. et al. (2014) 'VGLL4 functions as a new tumor suppressor in lung cancer by negatively regulating the YAP-TEAD transcriptional complex', *Cell Res* 24(3): 331-43.
Zhou, D., Zhang, Y., Wu, H., Barry, E., Yin, Y., Lawrence, E., Dawson, D., Willis, J. E., Markowitz, S. D., Camargo, F. D. et al. (2011) 'Mst1 and Mst2 protein kinases restrain intestinal stem cell proliferation and colonic tumorigenesis by inhibition of Yes-associated protein (Yap) overabundance', *Proc Natl Acad Sci U S A* 108(49): E1312-20.

Figures

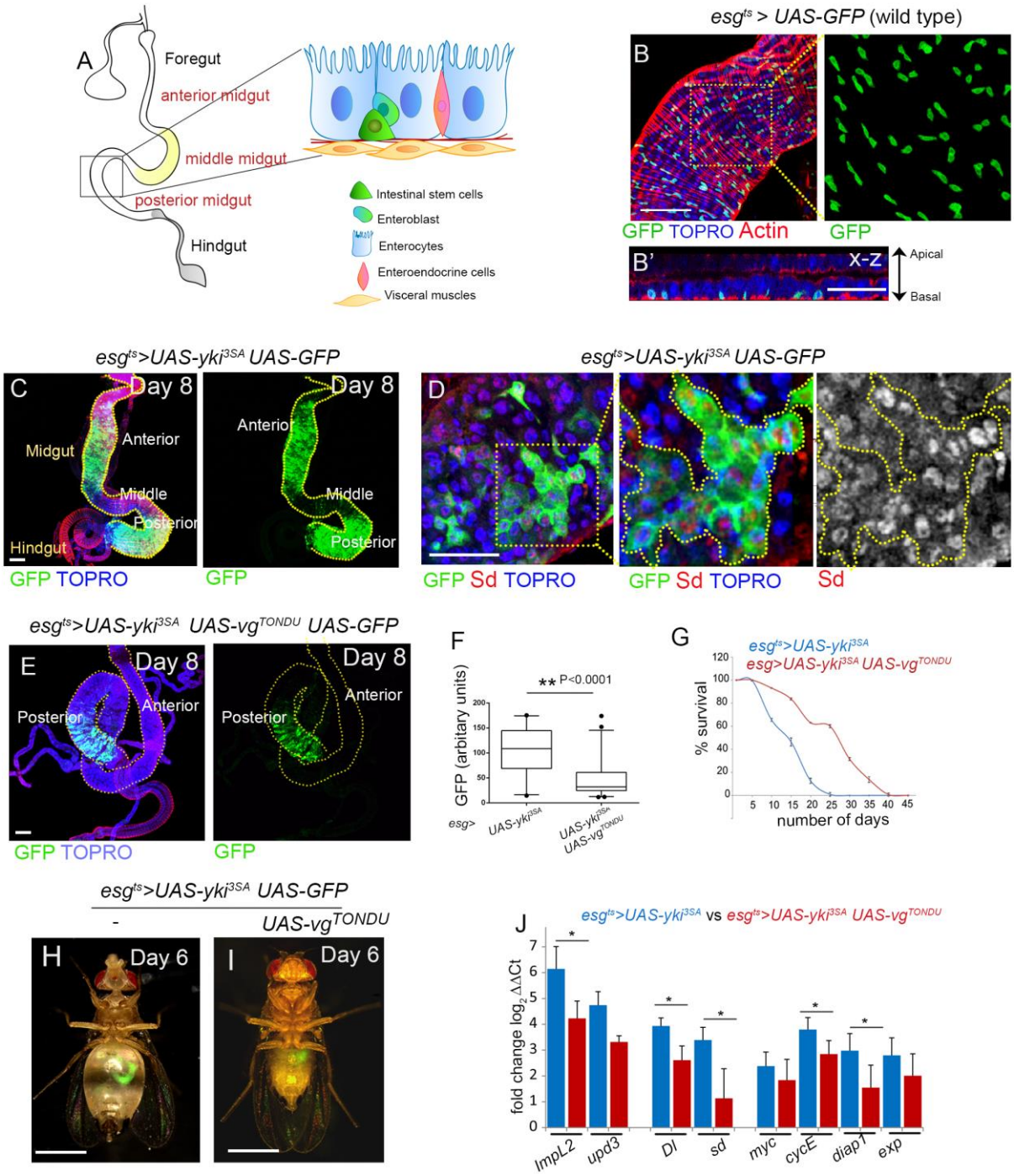

Figure 1. Expression of the TONDU peptide inhibits Yki-driven ISC tumors. (A) Schematic representation depicting the different cell types in the adult *Drosophila* gut. (B, B') *esg^{ts}>UAS-GFP* labels ISCs in the *Drosophila* midgut. (B) ISCs (marked by GFP) are interspersed throughout the gut. Overlying muscles are marked with F-Actin (red). (B') X-Z section displaying basally located ISCs (GFP). (C) *esg^{ts}>yki^{3SA}UAS-GFP* gut shows an

increase in ISC numbers. (D) *esg^{ts}>yki^{3SA}UAS-GFP* tumors show increase in Sd level. (E) Decrease in ISCs (marked by GFP) in the anterior and posterior midgut of *esg^{ts}>yki^{3SA} UAS-vg^{TONDU}* flies that coexpress the TONDU peptide. (F) Quantification of GFP in TONDU-expressing and non-expressing *esg^{ts}>yki^{3SA}*guts. (G) Increase in survival of *esg^{ts}>yki^{3SA}UAS-vg^{TONDU}* flies compared to *esg^{ts}>yki^{3SA}* (n=50 each genotype). (H) Abdominal bloating in *esg^{ts}>yki^{3SA}UAS-GFP* flies as seen on day 6 after tumor induction (n=19/25 are bloated). (I) *esg^{ts}>yki^{3SA} UAS-vg^{TONDU} UAS-GFP* flies display delay in bloating (n=14/25 are not bloated) as seen on day 6. (J) qPCR displaying the decrease in mRNA levels of candidate genes in TONDU-expressing flies. Data presented as mean ±SE; ∗ marks P≤ *0.025* for Student's t-test. Scale bars 100 µm in all, except B' and D: 50 µm, and H and I: 1mm.

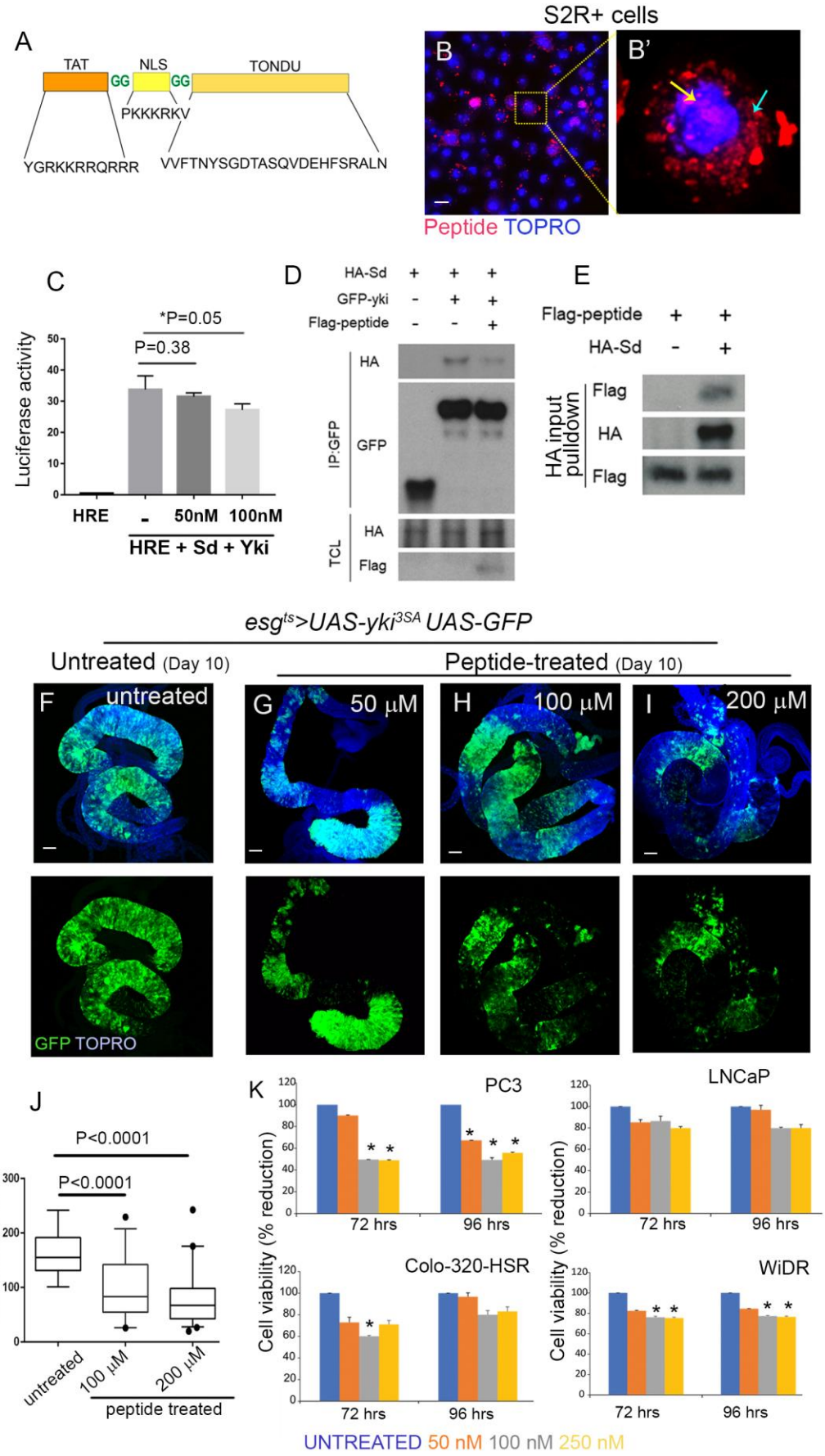

Figure 2. Synthetic TONDU peptide inhibits Yki-driven ISC tumors. (A) Representation of the synthetic TONDU peptide. (B-B') Nuclear localization of fluorescent-tagged (red) TONDU peptide in S2R+ cells. (B') Magnified view of the boxed area in B. TONDU-Peptide (red) in the nucleus (yellow arrow) and cytoplasm (blue arrow). (C) Decrease in HRE-Luciferase reporter activity in S2R+ cells when treated with TONDU peptide. (D-E) Immunoblots showing competitive binding of TONDU peptide to Yki-Sd complex (D). (E) Binding of TONDU peptide to Sd. (F-I) Guts from $esg^{ts}>yki^{3SA}$ flies fed on TONDU peptide. (F) Unfed (control), (G) 50 µM (n=10), (H) 100 µM (n=12) and (I) 200 µM (n=10). (J) Quantification of GFP in TONDU peptide-fed and -unfed $esg^{ts}>yki^{3SA}$flies. (K) Viability of cancer cells on treatment with TONDU peptide, as estimated using the Resazurin cell viability assay; ∗ marks P≤ *0.001* for Student's t-test. Scale bars: 10µm in B; 100 µm in F-I.

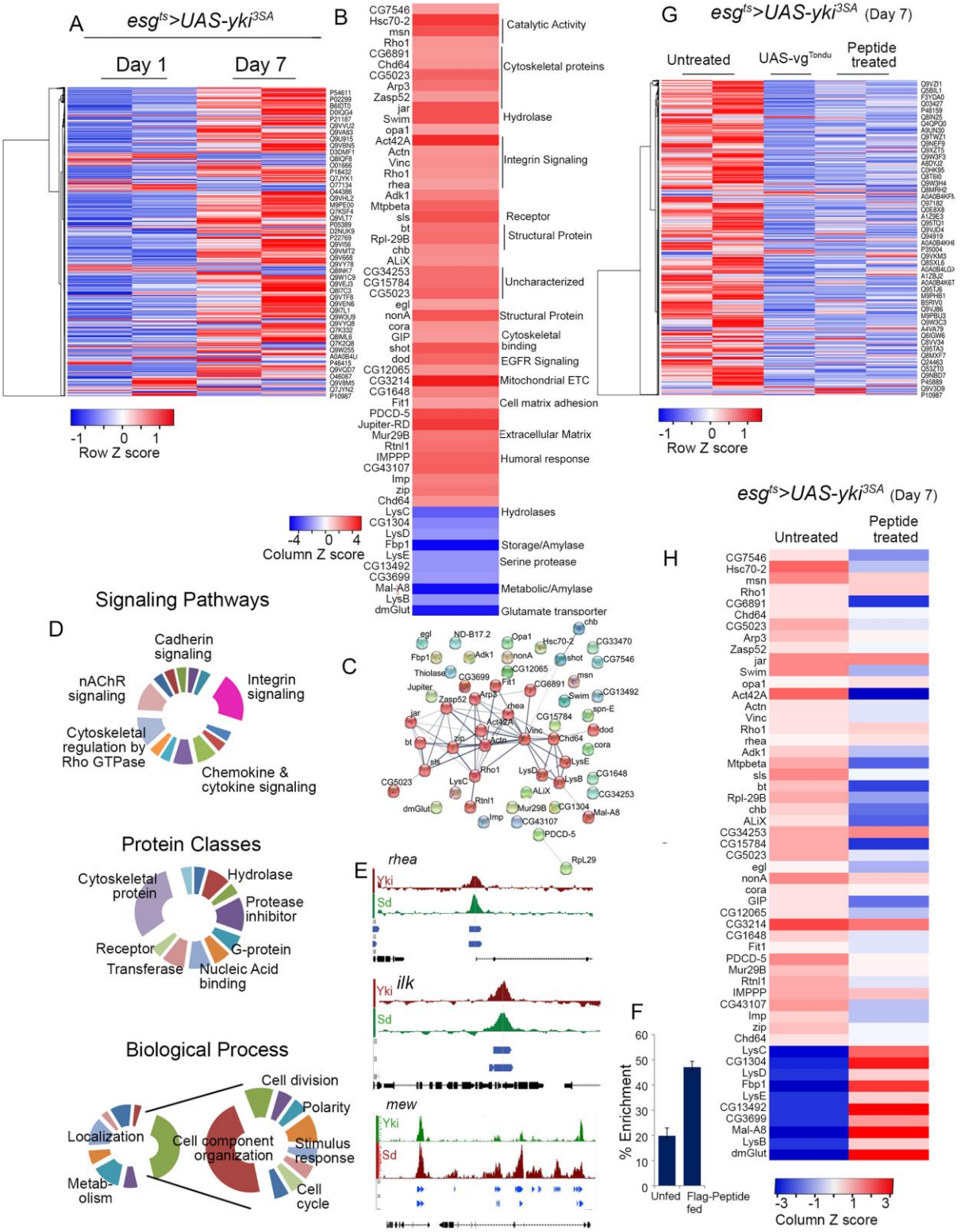

Figure 3. Comparative proteomic analysis of Yki-driven ISC tumors and tumors inhibited by the TONDU peptide: (A) Heat map displaying changes in protein levels in day 7 and day 1 of *esg^{ts}>yki^{3SA}* tumors. (B) 55 differentially (>±2 log$_2$fold, p=0.05) expressed proteins in day 7 *esg^{ts}>yki^{3SA}* tumors. (C) Protein-protein interaction (PPI) network of

enriched proteins (>$\log_2$ 2 fold) in *esg*^{ts}>*yki*^{3SA} tumors generated with STRING (Szklarczyk et al., 2019) representing 55 nodes and 63 edges (PPI enrichment p<0.0001). (D) Different Gene Ontology classes identified by PANTHER (Mi et al., 2007) in differentially expressed proteins between *esg*^{ts}>*yki*^{3SA}-day7 *versus* -day 1 tumor proteome. (E) Sd and Yki binding sites in the regulatory regions of select integrin pathway members as determined in (Nagaraj et al., 2012). (F) Percent enrichment for Sd-binding upstream of *mew* (αPS1) inferred by ChIP with anti-FLAG antibody. (G) Heat map displaying the effect of TONDU peptide on *esg*^{ts}>*yki*^{3SA} tumor proteome. (H) Heat map displaying change in levels of protein (>±2 fold in day 7 tumors) upon TONDU peptide treatment.

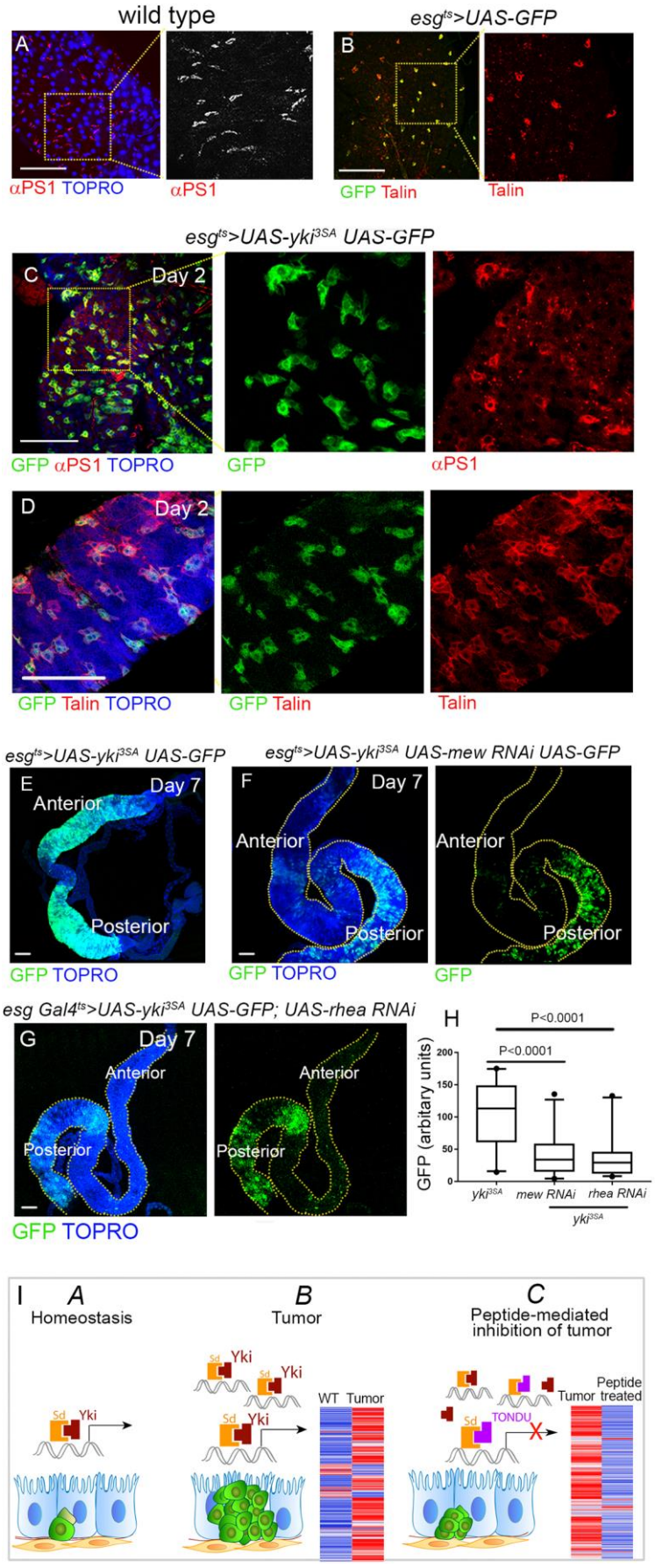

Figure 4. Loss of Integrin signaling inhibits growth of Yki-driven ISC tumors. (A-B) αPS1(A) and Talin (B) staining in *esg^{ts}>UAS-GFP* marked ISCs. (C-D) Overall increase in αPS1 (C) and Talin (D) in *esg^{ts}>yki^{3SA}* tumors. (E-G) Inhibition of Yki-driven tumors upon simultaneous down-regulation of αPS1 (*esg^{ts}>yki^{3SA} UAS-mew-RNAi*, n=9, F), or Talin (*esg^{ts}>yki^{3SA} UAS-rhea-RNAi*, n=9, G), when compared to similarly aged *esg^{ts}>yki^{3SA}* tumors (E and S5A, respectively). (H) Quantification of GFP from E, F and G. (I) Schematic of Yki-Sd mediated transcription in wild type guts (A); -in Yki tumor (B); and in –Yki tumors in the presence of the TONDU peptide (C). Scale bars 100 µm.

FIGURE S1

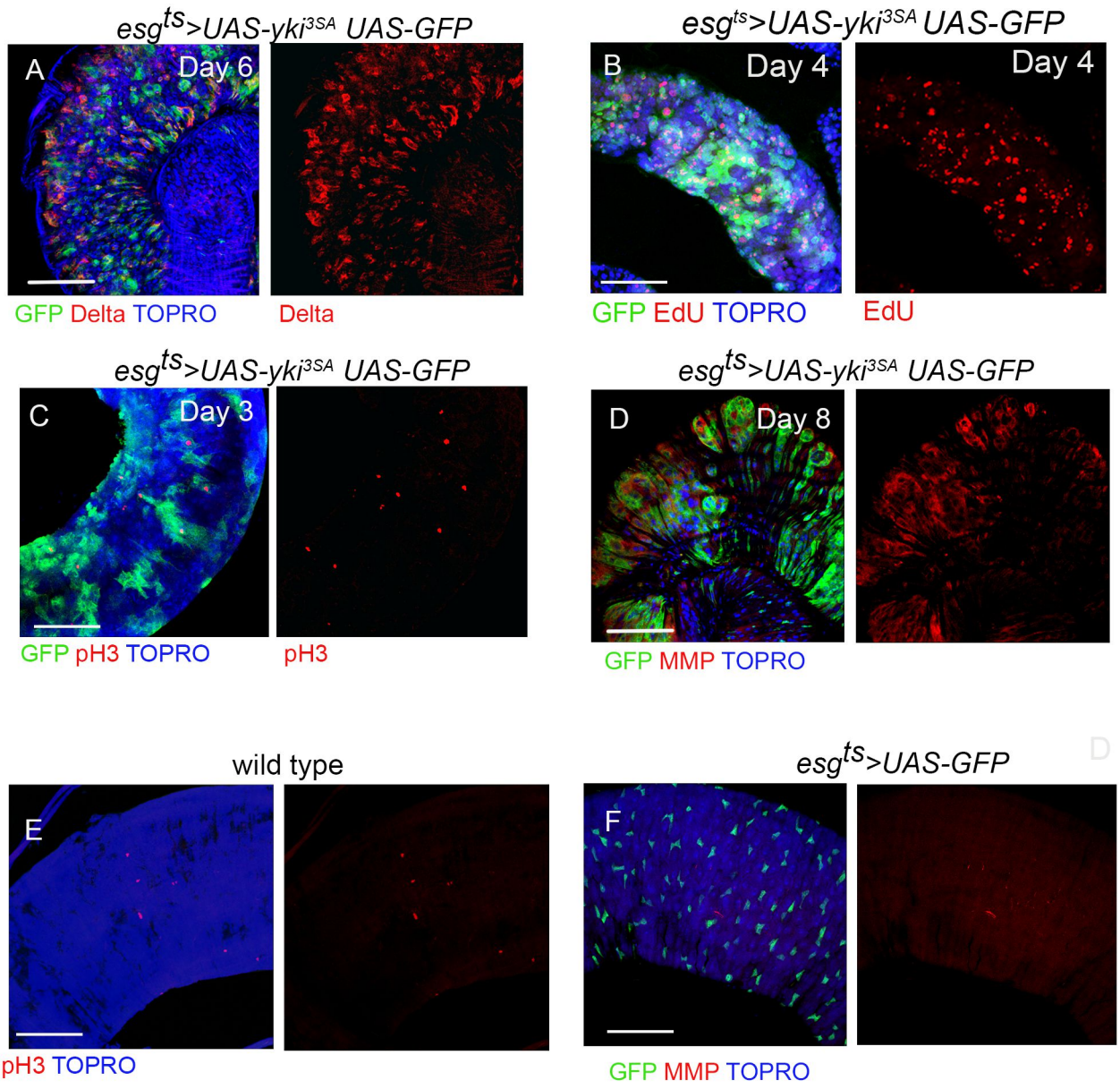

Figure S1. ISCs with constitutive gain of Yki display tumor phenotypes. (A-D) *esg^{ts}>yki^{3SA} UAS-GFP* tumors stained for the stem cell marker Delta (A), EdU uptake (B), Phospho-Histone (C), and MMP (D). (E-F) Wild type guts displaying Phospho-Histone (E), and MMP (F). Scale bars 100 µm.

FIGURE S2

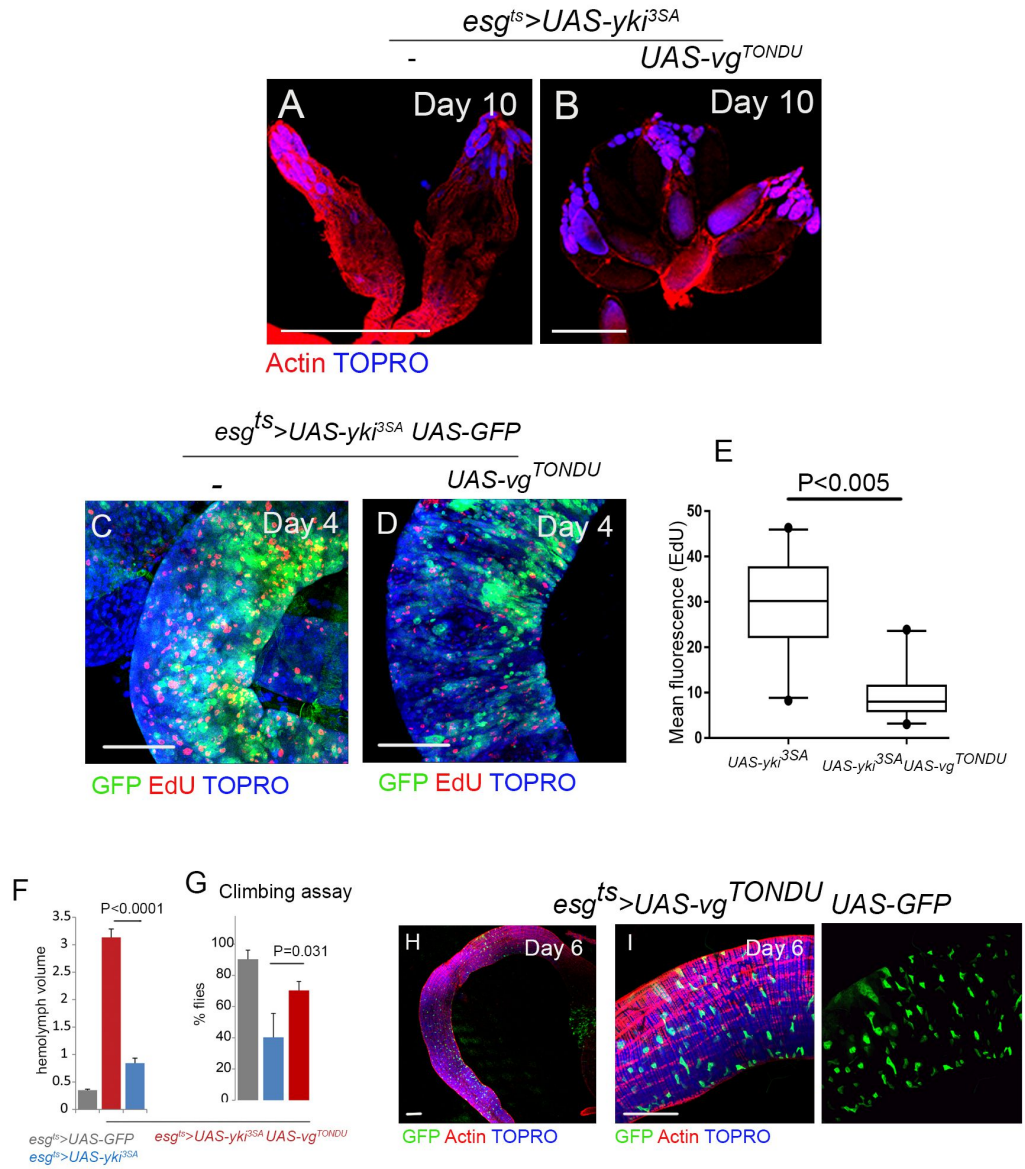

Figure S2. Overexpression of the TONDU peptide inhibits Yki-driven epithelial tumors. (A) Atrophy of ovaries in *esg^{ts}>yki^{3SA}* flies (n=21/25). (B) Improved morphology of ovaries in *esg^{ts}>yki^{3SA} UAS-vg^{TONDU}* flies (n=12/25). (C-E) Decrease in the number of proliferating cells detected by EdU (red) staining in *esg^{ts}>yki^{3SA} UAS-vg^{TONDU}* (D), compared to *esg^{ts}>yki^{3SA}* tumors (C). (E) Quantification of EdU fluorescence in C and D. (F) Decrease in hemolymph content (n=25) in *esg^{ts}>yki^{3SA} UAS-vg^{TONDU}* flies compared to *esg^{ts}>yki^{3SA}* flies on Day 7. (G) TONDU-expressing *esg^{ts}>yki^{3SA}* flies (n=35) suppress the loss of climbing activity seen in *esg^{ts}>yki^{3SA}* flies. (H-I) Expression of TONDU peptide in ISCs (*esg^{ts}>UAS-vg^{TONDU}*) does not affect ISC numbers. Scale bars 100 µm.

Figure S3

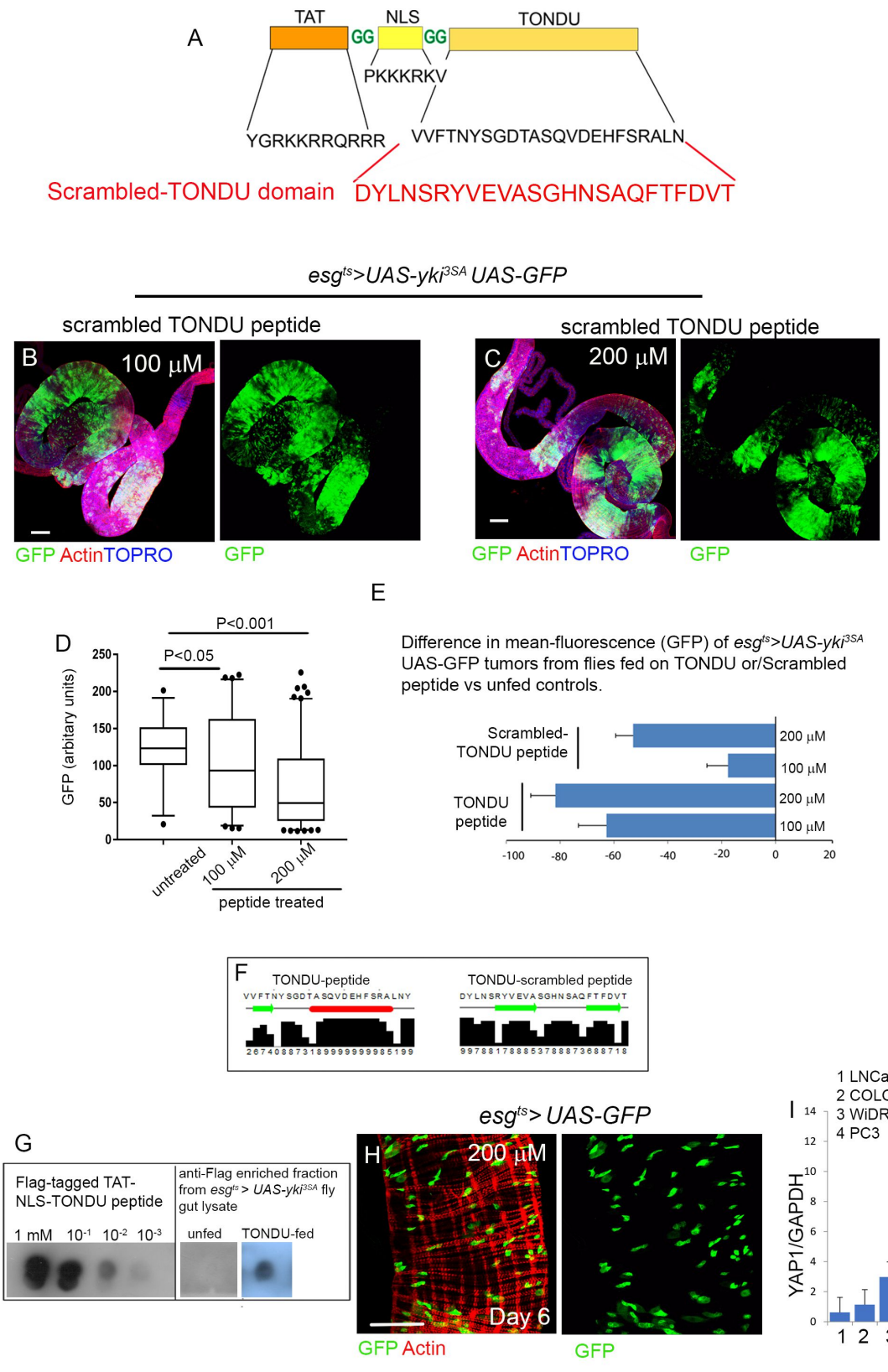

Figure S3. Scrambled-TONDU peptide fails to suppress Yki-driven ISC tumors. (A) Schematic representation of the scrambled-TONDU peptide. (B-D) The scrambled-TONDU peptide displays poor growth inhibition of $esg^{ts}>yki^{3SA}$ tumors (compare with Figure 2H and I). Box plot depicting GFP quantification in $esg^{ts}>yki^{3SA}$ tumors from flies fed on scrambled TONDU peptide (D). (E) Histogram displaying decrease in mean-GFP of $esg^{ts}>yki^{3SA}$ *UAS-GFP* tumors from flies fed with TONDU peptide or with scrambled-TONDU peptide, when compared to unfed controls. Note that the decrease is significantly more in TONDU peptide as compared to scrambled peptide fed tumors. (F) Secondary structures of the TONDU (left) and Scrambled-TONDU (right) as predicted by JPred (http://www.compbio.dundee.ac.uk/jpred/). Black bars represent the confidence estimate for the prediction (high value represents high confidence); helices are marked in red while green arrows depict sheets. (G) Dot blot for FLAG-tagged TONDU peptide using anti-FLAG antibody, on native peptide (different serial dilutions); and in cell lysate (right panel) from guts (n=25) of flies fed on 200 µM of FLAG-tagged TONDU peptide and unfed flies used as control. (H) Control ($esg^{ts}>$*UAS-GFP*) flies fed on 200 µM of TONDU peptide do not display changes in ISC numbers. (I) mRNA levels of *YAP1* in different human cancer cell lines as determined by qPCR. Scale bars 100 µm.

Figure S4

X-Y plot depicting correlation between proteome and transcripome of *esg*^{ts}>*yki*^{3SA} tumor

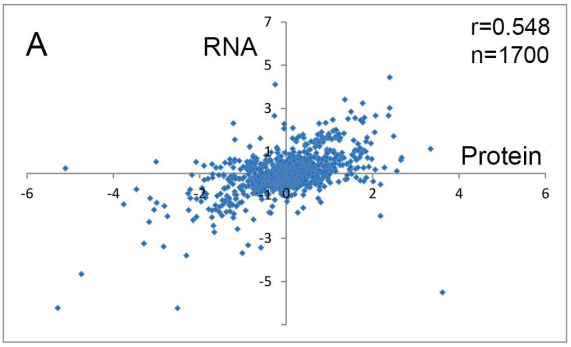

Scatter plot displaying fold change in individual proteins in *esg*^{ts}>*yki*^{3SA} tumors in presence of TONDU peptide

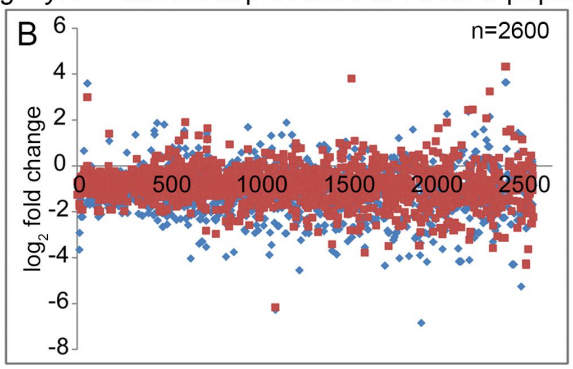

x axis: individual proteins
y axis: fold change

esg^{ts} >*yki*^{3SA} tumors from flies fed on TONDU peptide *versus* unfed controls.

esg^{ts}>*yki*^{3SA}; *UAS-vg*^{TONDU} *versus esg*^{ts}>*yki*^{3SA} tumors

X-Y plot depicting correlation between TONDU peptide-treated and TONDU peptide-expressed *esg*^{ts}>*yki*^{3SA} tumor proteome

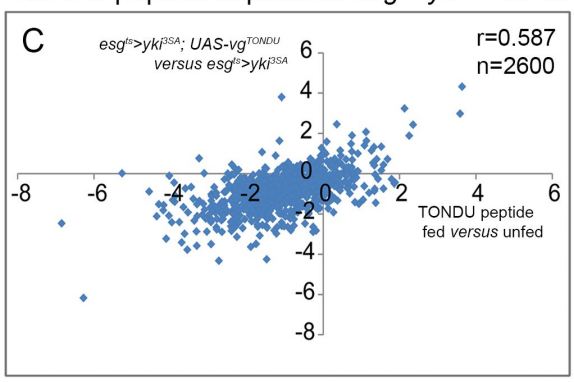

Figure S4. Comparison of the proteomes of TONDU peptide-treated ISC tumors and tumors with genetic gain of peptide. (A) X-Y correlation plot displaying Z-score comparison of log_2 fold change of genes in the proteome (current study) and transcriptome (Song et al., 2019) of $esg^{ts}>yki^{3SA}$ tumors. (B) Scatter plots displaying fold change (log_2) for individual proteins (x axis) in TONDU peptide-fed versus unfed $esg^{ts}>yki^{3SA}$ tumors (red); and for $esg^{ts}>yki^{3SA}$ *UAS-*vg^{TONDU} versus $esg^{ts}>yki^{3SA}$ tumors (blue). (C) X-Y correlation plot for B.

Figure S5

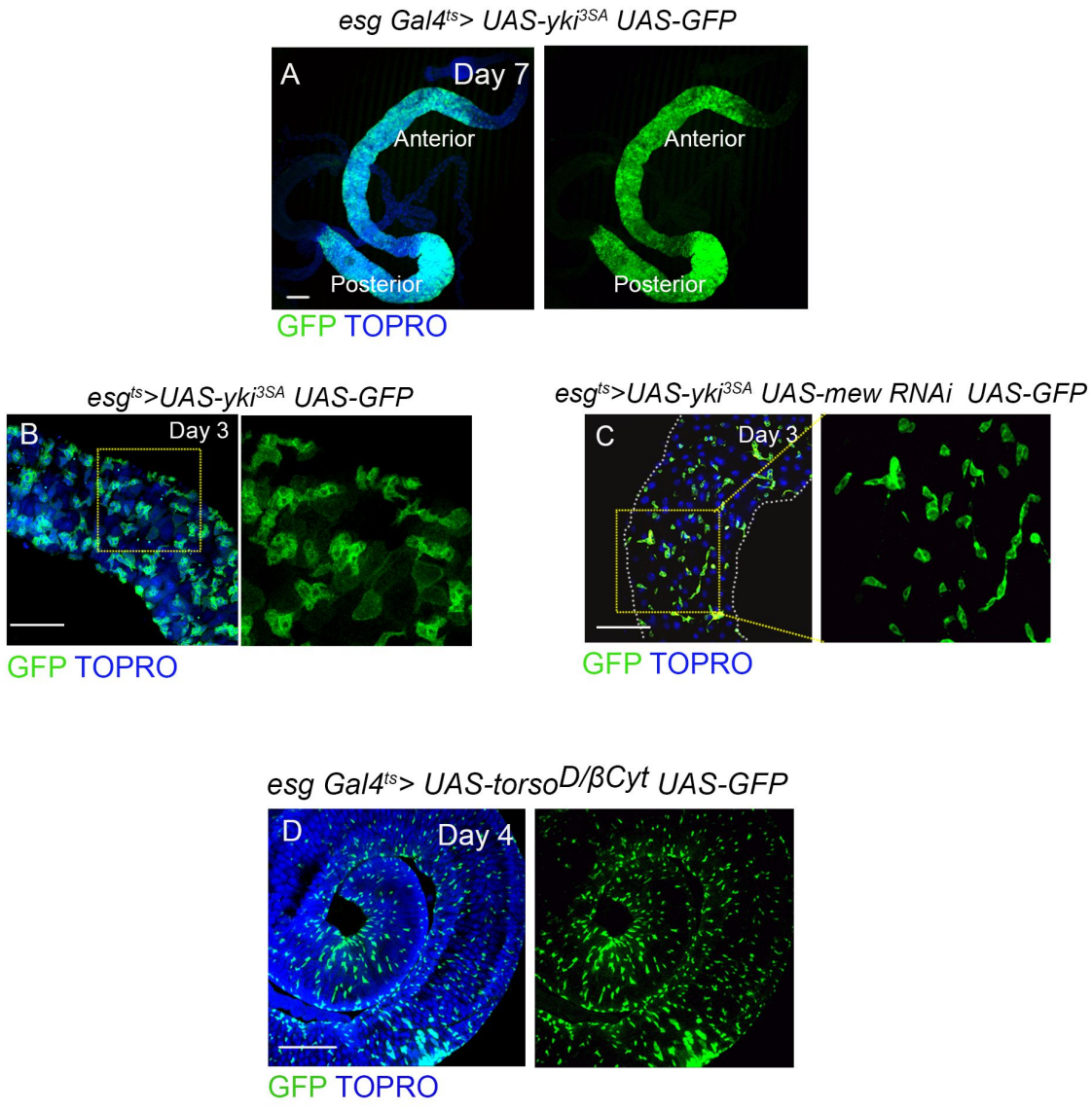

Figure S5. Loss of integrin signaling in Yki-driven ISC tumors. (A) *esg^{ts}>yki^{3SA}* tumors (day 7) control for *esg^{ts}>yki^{3SA} UAS-rhea RNAi* (see Fig. 4G). (B-C) Early *esg^{ts}>yki^{3SA} UAS-mew RNAi* tumors (day 3) display small ISC clusters (C) compared to similarly aged *esg^{ts}>^{yki3SA}* tumors (B). (D) Constitutive gain of integrin signaling in *esg^{ts}>UAS-torso$^{D/βCyt}$* as seen on day 4 of Gal4 activation. No aberrant increase in ISC numbers was observed. Scale bars 100 µm.

Table S1: List of proteins identied by unlabeled LC-MS/MS proteomic analysis of Yki-driven Intestinal Stem Cell (ISC) tumors in *Drosophila* adult midguts.

Click here to Download Table S1

Table S2: Proteins with significant fold change ($\geq \pm \log_2 2$, $p<0.05$) in day 7 versus day 1 of $esg^{ts}>yki^{3SA}$ driven ISC tumors.

Gene ID	Gene Symbol	Protein FDR Confidence: Combined	Master	UniProt Accession	Median *(Day 1)*	Median *(Day 7)*	Abundance Ratio: Day 7/ Day 1	Abundance Ratio (log2)	T-Test (P value)	# amino acis	MW [kDa]	# Peptides (Sequest HT)	Chromosome	Found in Sample Group: (Day 1)	Found in Sample Group: (Day 7)
FBgn0261276	*Opa1*	High	None	F0JAH2	74046.703	297394.711	4.016	**2.006**	**0.0048**	453	51.2	2	2R	Peak Found	High
FBgn0000562	*egl*	Medium	Master Protein Candidate	Q9W1K4	14056.321	57460.557	4.088	**2.031**	**0.0430**	1004	112.1	1	2R	Peak Found	High
FBgn0260442	*rhea*	High	Master Protein	Q960C2	67243.947	276212.477	4.108	**2.038**	**0.0264**	1601	171.2	26	3L	High	High
FBgn0035498	*Fit1*	High	Master Protein	Q9VZI3	394737.461	1640060.666	4.155	**2.055**	**0.0276**	708	80.4	6	3L	High	High
FBgn0035793	*CG7546*	High	Master Protein Candidate	M9PBU3	91147.313	390343.234	4.283	**2.098**	**0.0087**	1179	125.7	2	3L	High	High
FBgn0030955	*CG6891*	High	Master Protein Candidate	Q8MQZ6	100332.746	448638.875	4.472	**2.161**	**0.0323**	269	30.2	1	X	High	High
FBgn0013437	*copia*	High	Master Protein	P04146	581703.875	2664281.188	4.580	**2.195**	**0.0138**	1409	162.7	3		High	High
FBgn0265991	*Zasp52*	High	None	G3JX29	147506.977	678663.543	4.601	**2.202**	**0.0366**	651	70.9	3	2R	High	High
FBgn0015379	*dod*	High	Master Protein	P54353	10240.124	94620.563	9.240	**3.208**	**0.0451**	166	18.4	1	X	Peak Found	High
FBgn0000667	*Actn*	High	Master Protein Candidate	M9MS06	60172.696	284884.955	4.734	**2.243**	**0.0489**	895	103.8	4	X	Peak Found	High
FBgn0010434	*cora*	High	Master Protein Candidate	A0A0B4LFX4	469318.387	2248560.410	4.791	**2.260**	**0.0047**	1600	173.8	6	2R	High	High
FBgn0014020	*Rho1*	High	Master Protein	P48148	491985.963	2396139.059	4.870	**2.284**	**0.0177**	192	21.7	6	2R	Peak Found	High
FBgn0030052	*CG12065*	High	None	Q8MRM6	279747.601	1375997.625	4.919	**2.298**	**0.0460**	641	71.1	5	X	Peak Found	High
FBgn0053470	*CG33470; IM10; IMPPP*	High	Master Protein	Q8ML70	3874.029	38433.805	9.921	**3.310**	**0.0377**	257	28	1	2R	Peak Found	High
FBgn0035499	*Chd64*	High	None	M9PE30	6518473.696	32604473.558	5.002	**2.322**	**0.0003**	175	19.4	25	3L	High	High
FBgn0025352	*Mtpβ*	High	Master Protein	O77466	60337.865	605581.250	10.037	**3.327**	**0.0340**	469	50.6	1	2R	Peak Found	High
FBgn0086346	*ALiX*	High	Master Protein	Q9VB05	77987.759	397127.230	5.092	**2.348**	**0.0169**	836	92.5	2	3R	Peak Found	High
FBgn0260442	*rhea*	High	None	M9NDM3	1072195.987	5647432.310	5.267	**2.397**	**0.0350**	2169	235.1	31	3L	High	High
FBgn0004397	*Vinc*	High	Master Protein	X2JAB9	741152.635	3905646.674	5.270	**2.398**	**0.0224**	961	106.2	12	X	High	High
FBgn0021760	*chb*	High	Master Protein	Q9NBD7	31028.359	169383.656	5.459	**2.449**	**0.0329**	1491	165.5	2	3L	Peak Found	High
FBgn0262567	*CG43107*	High	Master Protein	D0IQC0	9607.135	107383.602	11.177	**3.483**	**0.0174**	63	6.8	1	2R	Peak Found	Peak Found
FBgn0013733	*shot*	High	Master Protein	A1Z9J3	28039.734	350253.043	12.491	**3.643**	**0.0138**	8805	988.9	2	2R	Peak Found	High
FBgn0033446	*CG1648*	High	Master Protein	Q7K2P3	775279.577	5030252.721	6.488	**2.698**	**0.0201**	230	23.8	18	2R	High	High
FBgn0262735	*Imp*	High	Master Protein	Q0KHU2	88808.606	580638.375	6.538	**2.709**	**0.0201**	631	69.4	3	X	Peak Found	High
FBgn0022709	*Adk1*	High	Master Protein Candidate	Q9VTV3	17311.554	113919.848	6.581	**2.718**	**0.0072**	201	21.9	1	3L	Peak Found	High
FBgn0086906	*sls*	High	None	R4UAY6	23315.416	308855.279	13.247	**3.728**	**0.0122**	662	74.6	2	3L	High	High
FBgn0010909	*msn*	Medium	None	Q7KV90	7461.706	102635.387	13.755	**3.782**	**0.0121**	1200	130.3	1	3L	Peak Found	High

FBgn0036580	*PDCD-5*	High	Master Protein	Q9VUZ8	11643.499	169815.949	14.585	**3.866**	**0.0111**	133	15.1	2	3L	Peak Found	Peak Found
FBgn0051901	*Mur29B*	Medium	Master Protein Candidate	Q8MS63	22220.121	166646.781	7.500	**2.907**	**0.0366**	339	35.7	1	2L	High	High
FBgn0265434	*zip*	High	None	A0A0B4JD95	3745790.734	28852286.631	7.703	**2.945**	**0.0010**	1964	226.6	67	2R	High	High
FBgn0005666	*bent*	High	None	O76281	284599.331	2219016.392	7.797	**2.963**	**0.0385**	6658	743	15	4	Peak Found	High
FBgn0262716	*Arp3; Arp66B*	High	Master Protein	P32392	91762.304	725246.529	7.904	**2.982**	**0.0397**	418	47	4	3L	High	High
FBgn0053113	*Rtnl1*	High	Master Protein Candidate	Q9VMV9	594076.854	5048772.010	8.499	**3.087**	**0.0238**	595	63.9	9	2L	High	High
FBgn0085282	*CG34253*	High	Master Protein	A8JNV2	26812.808	228363.336	8.517	**3.090**	**0.0221**	112	12.5	1	3L	Peak Found	High
FBgn0265434	*zip*	High	None	J7JVR0	1687952.657	14541350.003	8.615	**3.107**	**0.0003**	1425	164.4	39	2R	High	High
FBgn0016726	*RpL29*	High	Master Protein	B7FNL1	732637.288	6371885.220	8.697	**3.121**	**0.0452**	85	10	6	2R	High	High
FBgn0029766	*CG15784*	High	Master Protein	Q9W4C1	151556.702	1363172.164	8.994	**3.169**	**0.0261**	554	62.3	5	X	High	High
FBgn0038774	*CG5023*	High	Master Protein	Q9I7J0	580277.645	5744084.078	9.899	**3.307**	**0.0314**	169	19.1	9	3R	High	High
FBgn0001217	*Hsc70-2*	High	Master Protein	P11146	34573.184	694860.797	20.098	**4.329**	**0.0135**	633	69.7	3	3R	Peak Found	High
FBgn0051363	*CG31363*	High	Master Protein	B5RJ67	30460.900	612434.938	20.106	**4.330**	**0.0112**	230	24.4	1	3R	Peak Found	High
FBgn0000043	*Act42A*	High	Master Protein	P02572	13317.133	326000.129	24.480	**4.614**	**0.0155**	376	41.8	37	2R	Peak Found	High
FBgn0004227	*nonA*	High	Master Protein	Q8IR16	51621.380	664389.951	12.870	**3.686**	**0.0092**	742	81.9	5	X	High	High
FBgn0011225	*jar*	High	Master Protein	Q01989	32407.746	421589.398	13.009	**3.701**	**0.0170**	1253	143.2	6	3R	Peak Found	High
FBgn0034709	*CG3074; Swim*	High	Master Protein	Q7JWQ7	582800.990	7699009.721	13.210	**3.724**	**0.0014**	431	48.8	11	2R	High	High
FBgn0031436	*CG3214; ND-B17.2*	High	Master Protein	Q9VQD7	13005.392	404752.090	31.122	**4.960**	**0.0032**	142	16.8	2	2L	High	High
FBgn0000639	*Fbp1*	High	Master Protein Candidate	M9PFK6	2941545.182	75592.226	0.026	**-5.282**	**0.0184**	1027	119.4	15	3L	High	Peak Found
FBgn0033297	*Mal-A8*	High	Master Protein Candidate	H5V882	145483.008	4449.611	0.031	**-5.031**	**0.0020**	597	68.1	1	2R	High	Peak Found
FBgn0010497	*dmGlut; l(2)01810*	Medium	Master Protein Candidate	Q95R95	217644.070	7972.730	0.037	**-4.771**	**0.0143**	165	17.7	1	2L	High	Peak Found
FBgn0004426	*LysC*	High	None	P83971	1020142.977	101441.592	0.099	**-3.330**	**0.0171**	140	15.6	2	3L	High	Peak Found
FBgn0031141	*CG1304*	High	None	Q9VRD1	1379758.828	251684.488	0.182	**-2.455**	**0.0240**	260	27.8	1	X	High	High
FBgn0004427	*LysD*	High	Master Protein Candidate	P83972	2366383.414	523926.295	0.221	**-2.175**	**0.0126**	140	15.6	3	3L	High	High
FBgn0004425	*LysB*	High	Master Protein Candidate	Q08694	2366383.414	523926.295	0.221	**-2.175**	**0.0126**	140	15.6	3	3L	High	High
FBgn0004428	*LysE*	High	Master Protein	P37159	2366383.414	523926.295	0.221	**-2.175**	**0.0126**	140	15.5	3	3L	High	High
FBgn0034662	*CG13492*	High	Master Protein	Q8MLU9	1715613.215	393704.303	0.229	**-2.124**	**0.0428**	2979	321.1	12	2R	High	High
FBgn0040349	*CG3699*	High	Master Protein Candidate	Q9U1L2	6207241.123	1490634.446	0.240	**-2.058**	**0.0024**	251	26	12	X	High	High

Table S3: Interacting partners belonging to the Hippo pathway for proteins with ≥$\log_2$ 2 fold change in *esg^{ts}>yki^{3SA}* driven ISC tumors.

. Protein	Fold change ($\log_2$ fold)	T Test P value	LC-MS/MS Proteomics	Uniprot	$Hippo protein-protein interaction network	
					Protein-and-Hippo pathway member	Score
Cora	2.2604	0.0047	High	A0A0B4LFX4	Cora ←→Ft	1*
Mtb-β	3.3272	0.0340	Peak Found	O77466	Mtb-β ←→Ft	0.99*
Msn	3.7819	0.0121	Peak Found	Q7KV90	Msn ←→Ft	1*
nonA	3.6860	0.0092	High	Q8IR16	nonA ←→Ex	0.82*
Jar	3.7014	0.0170	Peak Found	Q01989	Jar ←→Wts	0.89*
Talin	2.0383	0.0264	High	Q960C2	Talin ←→Yki	0.33
Vinc	2.2184	0.0188	High	Q24584	Vinc ←→Ft	0.36
Chd64	2.3225	0.0003	High	M9PE30	Chd64 ←→Yki	0.01
Mtb-β	3.3272	0.0340	Peak Found	O77466	Mtb-β ←→Wts	0.1
Arp3	2.9825	0.0397	High	P32392	Arp3 ←→Wts	0.21
Rtnl1	3.0872	0.0238	High	Q9VMV9	Rtnl1 ←→Ft	0.38
nonA	3.6860	0.0092	High	Q8IR16	nonA ←→Wts	0.28

$Kwon *et al.* (Kwon et al., 2013). *Statistically significant interactions

Table S4: Gene Ontology (GO) analysis of enriched proteins in *esg^{ts}>yki^{3SA}* driven ISC tumors.

MOLECULAR FUNCTION		$GO classes	Gene Numbers	% representation	% representation
	1	binding (GO:0005488)	7	19.40%	29.20%
	2	structural molecule activity (GO:0005198)	6	16.70%	25.00%
	3	molecular function regulator (GO:0098772)	1	2.80%	4.20%
	4	catalytic activity (GO:0003824)	10	27.80%	41.70%
BIOLOGICAL PROCESS					
	1	response to stimulus (GO:0050896)	2	5.60%	7.40%
	2	cellular process (GO:0009987)	11	30.60%	40.70%
	3	multicellular organismal process (GO:0032501)	1	2.80%	3.70%
	4	metabolic process (GO:0008152)	6	16.70%	22.20%
	5	biological regulation (GO:0065007)	2	5.60%	7.40%
	6	localization (GO:0051179)	4	11.10%	14.80%
	7	biological adhesion (GO:0022610)	1	2.80%	3.70%
CELLULAR COMPONENT					
	1	organelle (GO:0043226)	9	25.00%	45.00%
	2	extracellular region (GO:0005576)	1	2.80%	5.00%
	3	cell (GO:0005623)	10	27.80%	50.00%
PROTEIN CLASSES					
	1	transmembrane receptor regulatory/adaptor protein (PC00226)	1	2.80%	4.20%
	2	hydrolase (PC00121)	5	13.90%	20.80%
	3	cell junction protein (PC00070)	1	2.80%	4.20%
	4	enzyme modulator (PC00095)	6	16.70%	25.00%
	5	nucleic acid binding (PC00171)	3	8.30%	12.50%

	6	transferase (PC00220)	1	2.80%	4.20%
	7	receptor (PC00197)	1	2.80%	4.20%
	8	cytoskeletal protein (PC00085)	5	13.90%	20.80%
	9	structural protein (PC00211)	1	2.80%	4.20%
PATHWAYS					
	1	Gonadotropin-releasing hormone receptor pathway (P06664)	1	2.80%	4.30%
	2	Cadherin signaling pathway (P00012)	1	2.80%	4.30%
	3	De novo purine biosynthesis (P02738)	1	2.80%	4.30%
	4	Axon guidance mediated by Slit/Robo (P00008)	1	2.80%	4.30%
	5	Apoptosis signaling pathway (P00006)	1	2.80%	4.30%
	6	Integrin signalling pathway (P00034)	5	13.90%	21.70%
	7	Angiogenesis (P00005)	1	2.80%	4.30%
	8	Alzheimer disease-presenilin pathway (P00004)	1	2.80%	4.30%
	9	Inflammation mediated by chemokine and cytokine signaling pathway (P00031)	2	5.60%	8.70%
	10	Huntington disease (P00029)	1	2.80%	4.30%
	11	Parkinson disease (P00049)	1	2.80%	4.30%
	12	Ras Pathway (P04393)	1	2.80%	4.30%
	13	Cytoskeletal regulation by Rho GTPase (P00016)	3	8.30%	13.00%
	14	Nicotinic acetylcholine receptor signaling pathway (P00044)	3	8.30%	13.00%

[$]GO enrichment was determined using PANTHER (http://www.pantherdb.org/).

Table S5: Status of integrin pathway members in *esg*^{ts}>*yki*^{3SA} driven ISC tumors.

Gene ID	Pathway member	Fly base ID	**Proteomics** (log_2 fold). Current study	[$]**RNAseq** ($log_2$ fold)
scb/aPS3	Integrin receptor	FBgn0003328	2.6069 (UP, P=0.270)	3.2797 (UP)
rhea	Adaptor	FBgn0260442	2.3970 (UP, P=0.035)	2.4646 (UP)
Ilk	Kinase and Scaffold protein	FBgn0028427	2.0724 (UP, P=0.056)	1.6871 (UP)
Pax	Scaffold protein	FBgn0041789	6.0551 (UP, P=0.051)	1.6507 (UP)
Vinc	Scaffold protein	FBgn0004397	2.3977 (UP, P=0.022)	2.8706 (UP)
vkg	Basemen Membrane	FBgn0016075	1.8255 (UP, P=0.014)	2.5527 (UP)
Rho1	GTPase	FBgn0014020	2.2840 (UP, P=0.018)	2.3794 (UP)
Act42A	Cytoskeleton	FBgn0000043	4.6013 (UP, P=0.1934)	5.1188 (UP)
mew/alpha-PS1	Integrin receptor	FBgn0004456	not found	3.3184 (UP)
mys/betaPS1	Integrin receptor	FBgn0004657	not found	3.7469 (UP)
if/alphaPS2,	Integrin receptor	FBgn0001250	not found	0.3507
ltgbn/ltgbetanu	Integrin receptor	FBgn0010395	not found	0.1434
LanA	Ligand	FBgn0002526	not found	3.0021 (UP)
wb/LanA1	Ligand	FBgn0261563	not found	2.0211 (UP)
LanB1	Ligand	FBgn0261800	not found	2.4286 (UP)

[$] Song *et al.* (Song et al., 2019).

Table S6: Putative Yki-Sd binding sites[$] in regulatory regions of genes found enriched in *esg^{ts}>yki^{3SA}* tumors.

Fly base ID	Gene Symbol	Fold enrichment in *esg^{ts}>yki^{3SA}* tumors	Chromosome	[$]Yki-Sd binding site from TSS
FBgn0261276	*opa1*	2.0059	2R	-690*
FBgn0000562	*egl*	2.0314	2R	-9.5
FBgn0035498	*Fit1*	2.0548	3L	-317
FBgn0035793	*CG7546*	2.0985	3L	-533, 193
FBgn0030955	*CG6891*	2.1608	X	-682; -316; 456
FBgn0015379	*dod*	3.2079	X	-29.5
FBgn0000667	*Actn*	2.2432	X	233.5
FBgn0010434	*cora*	2.2604	2R	346.5
FBgn0014020	*Rho1*	2.2840	2R	22.5; 1058.5
FBgn0030052	*CG12065*	2.2983	X	87; 647.5
FBgn0035499	*Chd64*	2.3225	3L	57.5
FBgn0025352	*Mtpbeta*	3.3272	2R	-129
FBgn0021760	*chb*	2.4486	3L	-100; 92; 841
FBgn0013733	*shot*	3.6429	2R	94; -421.5; -1118.5; 7211; 839; 503; -114.5
FBgn0033446	*CG1648*	2.6978	2R	1867
FBgn0010909	*msn*	3.7819	3L	446; -30.5
FBgn0053113	*Rtnl1*	3.0872	2L	-599.5; -308.5; -1035.5; 90.5
FBgn0016726	*Rpl-29B*	3.1205	2R	-77
FBgn0000043	*Act42A*	4.6135	2R	-52; -365
FBgn0011225	*jar*	3.7014	3R	-562.5
FBgn0028427	*ilk*	2.0724	3L	-4.5
FBgn0041789	*Pax*	6.0551	2L	-19
FBgn0004397	*vinc*	2.3977	X	64.5; -614
FBgn0004456	*mew*	not found	X	-185
FBgn0004657	*alphaPS2*	not found	X	630.5; 1586; 1995.5
FBgn0010395	*Itgbeta nu*	not found	2L	-110
FBgn0002526	*lanA*	not found	3L	-569.5; -1244

[$]Nagaraj *et al.* (Nagaraj et al., 2012).

Table S7: Change in levels of proteins in TONDU peptide-treated *esg^{ts}>yki^{3SA}* driven ISC tumors.

				TREATED	
Fly base ID	Gene symbol	FDR confidence	UniProt Accession	Abundance Ratio.	T-Test (*p* value)
FBgn0261276	*opa1*	High	F0JAH2	-0.9677	0.0612
FBgn0000562	*egl*	Medium	Q9W1K4	Not found	Not found
FBgn0260442	*rhea*	High	Q960C2	-0.9850	0.6182
FBgn0035498	*Fit1*	High	Q9VZI3	-1.3108	0.4323
FBgn0035793	*CG7546*	High	M9PBU3	-1.9655	0.0057
FBgn0030955	*CG6891*	High	Q8MQZ6	-2.5940	0.0034
FBgn0013437	*GIP*	High	P04146	-2.1634	0.0034
FBgn0265991	*Zasp52*	High	G3JX29	-1.2146	0.1208
FBgn0015379	*dod*	High	P54353	not found	Not found
FBgn0000667	*Actn*	High	M9MS06	-1.3641	0.0427
FBgn0010434	*cora*	High	A0A0B4LFX4	-1.0595	0.0051
FBgn0014020	*Rho1*	High	P48148	-0.8551	0.0536

FBgn0030052	*CG12065*	High	Q8MRM6	-1.5401	0.0876
FBgn0053470	*CG33470; IM10; IMPPP*	High	Q8ML70	-0.7563	0.4986
FBgn0035499	*Chd64*	High	M9PE30	-1.2033	0.0076
FBgn0025352	*Mtpbeta*	High	O77466	-2.3300	0.0139
FBgn0086346	*ALiX*	High	Q9VB05	-2.3246	0.0151
FBgn0260442	*rhea*	High	M9NDM3	-1.2592	0.0478
FBgn0004397	*Vinc*	High	X2JAB9	-1.3361	0.0365
FBgn0021760	*chb*	High	Q9NBD7	-2.1663	0.0263
FBgn0262567	*CG43107*	High	D0IQC0	-1.6068	0.1094
FBgn0013733	*shot*	High	A1Z9J3	not found	Not found
FBgn0033446	*CG1648*	High	Q7K2P3	-1.2957	0.0316
FBgn0262735	*Imp*	High	Q0KHU2	-1.6114	0.0313
FBgn0022709	*Adk1*	High	Q9VTV3	-1.5700	0.0068
FBgn0086906	*sls*	High	R4UAY6	-1.2668	0.0439
FBgn0010909	*msn*	Medium	Q7KV90	-0.9091	0.0273
FBgn0036580	*PDCD-5*	High	Q9VUZ8	-1.1028	0.3096
FBgn0051901	*Mur29B*	Medium	Q8MS63	-1.0776	0.0244
FBgn0265434	*zip*	High	A0A0B4JD95	-1.1648	0.0140
FBgn0005666	*bt*	High	O76281	-2.5538	0.0038
FBgn0262716	*Arp3; Arp66B*	High	P32392	-1.1503	0.0234
FBgn0053113	*Rtnl1*	High	Q9VMV9	-1.2851	0.0129
FBgn0085282	*CG34253*	High	A8JNV2	-0.4406	0.0846
FBgn0265434	*zip-RC*	High	J7JVR0	-1.1466	0.0063
FBgn0016726	*Rpl-29B*	High	B7FNL1	-1.8229	0.1047
FBgn0029766	*CG15784*	High	Q9W4C1	-2.6531	0.0395
FBgn0038774	*CG5023*	High	Q9I7J0	-1.3464	0.0059
FBgn0001217	*Hsc70-2*	High	P11146	-1.5196	0.0343
FBgn0051363	*Jupiter-RD*	High	B5RJ67	not found	not found
FBgn0000043	*Act42A*	High	P02572	-3.6540	0.0297
FBgn0004227	*nonA*	High	Q8IR16	-0.8528	0.0079
FBgn0011225	*jar*	High	Q01989	-0.3926	0.4731
FBgn0034709	*CG3074; Swim*	High	Q7JWQ7	-1.6677	0.0054
FBgn0031436	*CG3214; ND-B17.2*	High	Q9VQD7	-0.3077	0.4512

REFERENCES

Kwon, Y., Vinayagam, A., Sun, X., Dephoure, N., Gygi, S. P., Hong, P. and Perrimon, N. (2013). The Hippo signaling pathway interactome. *Science* **342**, 737-40.

Nagaraj, R., Gururaja-Rao, S., Jones, K. T., Slattery, M., Negre, N., Braas, D., Christofk, H., White, K. P., Mann, R. and Banerjee, U. (2012). Control of mitochondrial structure and function by the Yorkie/YAP oncogenic pathway. *Genes Dev* **26**, 2027-37.

Song, W., Kir, S., Hong, S., Hu, Y., Wang, X., Binari, R., Tang, H. W., Chung, V., Banks, A. S., Spiegelman, B. et al. (2019). Tumor-Derived Ligands Trigger Tumor Growth and Host Wasting via Differential MEK Activation. *Dev Cell* **48**, 277-286 e6.